Human peroxiredoxin 6 is essential for malaria parasites and provides a host-based drug target

Matthias Paulus Wagner, Pauline Formaglio, Olivier Gorgette, Jerzy Michal Dziekan, Christèle Huon, Isabell Berneburg, Stefan Rahlfs, Jean-Christophe Barale, Sheldon I Feinstein, Aron B Fisher, et al.

Cell Reports

Article

Human peroxiredoxin 6 is essential for malaria parasites and provides a host-based drug target

Graphical abstract

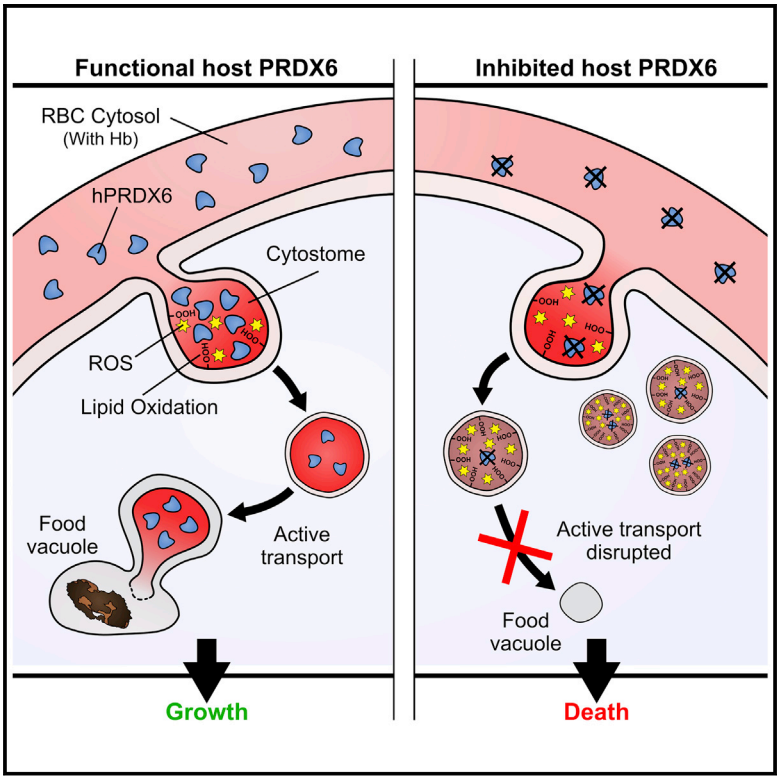

Authors

Matthias Paulus Wagner, Pauline Formaglio, Olivier Gorgette, ..., Rogerio Amino, Lhousseine Touqui, Chetan E. Chitnis

Correspondence

chetan.chitnis@pasteur.fr

In brief

Wagner et al. find that *Plasmodium falciparum* blood stages internalize human PRDX6, which repairs lipid-peroxidation damage. PRDX6 inhibitors prevent lipid repair and kill the parasite. Co-treatment of artemisinin-resistant strains with PRDX6 inhibitors and artemisinin restores susceptibility to artemisinin. PRDX6 thus provides a promising host-based target for anti-malaria drug development.

Highlights

- Human peroxiredoxin 6 (PRDX6) is internalized by *P. falciparum* blood stages
- Inhibition of host PRDX6 causes lethal lipid-peroxidation damage in the parasite
- Co-treatment with artemisinin and PRDX6 inhibitors overcomes artemisinin resistance
- Targeting of a host enzyme like PRDX6 may prevent development of drug resistance

Wagner et al., 2022, Cell Reports *39*, 110923
June 14, 2022
https://doi.org/10.1016/j.celrep.2022.110923

CellPress

Cell Reports

CellPress
OPEN ACCESS

Article

Human peroxiredoxin 6 is essential for malaria parasites and provides a host-based drug target

Matthias Paulus Wagner,[1] Pauline Formaglio,[2] Olivier Gorgette,[3] Jerzy Michal Dziekan,[4] Christèle Huon,[1] Isabell Berneburg,[5] Stefan Rahlfs,[5] Jean-Christophe Barale,[6,7] Sheldon I. Feinstein,[8] Aron B. Fisher,[8,9] Didier Ménard,[10,11] Zbynek Bozdech,[4] Rogerio Amino,[2] Lhousseine Touqui,[12,13] and Chetan E. Chitnis[1,14,*]

[1]Institut Pasteur, Université de Paris, Malaria Parasite Biology and Vaccines Unit, Paris, France
[2]Institut Pasteur, Université de Paris, Malaria Infection and Immunity Unit, Paris, France
[3]Institut Pasteur, Department of Cell Biology and Infection, Centre for Innovation and Technological Research, Ultrastructural Bioimaging Unit, Paris, France
[4]School of Biological Sciences, Nanyang Technological University, Singapore, Singapore
[5]Biochemistry and Molecular Biology, Interdisciplinary Research Centre, Justus Liebig University Giessen, Giessen, Germany
[6]Institut Pasteur, Université de Paris, CNRS UMR 3528, Structural Microbiology Unit, Paris, France
[7]Institut Pasteur, Pasteur International Unit, Pasteur International Network, Malaria Translational Research Unit, Phnom Penh, Cambodia and Paris, France
[8]Peroxitech, Inc., Philadelphia, PA, USA
[9]Institute for Environmental Medicine, Department of Physiology, University of Pennsylvania Perelman School of Medicine, Philadelphia, PA, USA
[10]Institut Pasteur, Université de Paris, INSERM U1201, Malaria Genetics and Resistance Unit, Paris, France
[11]Dynamics of Host-Pathogen Interactions, EA 7292, IPPTS, Strasbourg University, Strasbourg, France
[12]Cystic Fibrosis, Physiopathology and Phenogenomics, INSERM Unit 938, Saint-Antoine, Paris, France
[13]Institut Pasteur, Université de Paris, Laboratory of Cystic Fibrosis and Chronic Bronchopathies, Paris, France
[14]Lead contact
*Correspondence: chetan.chitnis@pasteur.fr
https://doi.org/10.1016/j.celrep.2022.110923

SUMMARY

The uptake and digestion of host hemoglobin by malaria parasites during blood-stage growth leads to significant oxidative damage of membrane lipids. Repair of lipid peroxidation damage is crucial for parasite survival. Here, we demonstrate that *Plasmodium falciparum* imports a host antioxidant enzyme, peroxiredoxin 6 (PRDX6), during hemoglobin uptake from the red blood cell cytosol. PRDX6 is a lipid-peroxidation repair enzyme with phospholipase A_2 (PLA_2) activity. Inhibition of PRDX6 with a PLA_2 inhibitor, Darapladib, increases lipid-peroxidation damage in the parasite and disrupts transport of hemoglobin-containing vesicles to the food vacuole, causing parasite death. Furthermore, inhibition of PRDX6 synergistically reduces the survival of artemisinin-resistant parasites following co-treatment of parasite cultures with artemisinin and Darapladib. Thus, PRDX6 is a host-derived drug target for development of antimalarial drugs that could help overcome artemisinin resistance.

INTRODUCTION

The mosquito-borne apicomplexan parasite *Plasmodium falciparum* was responsible for about 241 million malaria cases in 2020 that led to an estimated 627,000 deaths (WHO, 2021). Malaria thus remains a major public-health problem in the tropical world. All clinical symptoms of malaria are attributed to the blood stage of the parasite's life cycle where *P. falciparum* invades and multiplies within host red blood cells (RBCs). Resistance to the current state-of-the-art anti-malarial drug artemisinin (ART) in *P. falciparum*, which was first reported in Southeast Asia in the early 2000s (Noedl et al., 2008) and has now been detected in sub-Saharan Africa (Balikagala et al., 2021; Uwimana et al., 2021), poses a major threat to malaria control and elimination efforts. Mechanistically, *P. falciparum* attains ART resistance by reducing the uptake of host RBC hemoglobin, which in turn leads to lower oxidative-stress levels and prevents activation of ART, enabling parasite survival (Birnbaum et al., 2020). Understanding the mechanisms for hemoglobin uptake and oxidative-stress management by the parasite could provide strategies to overcome ART resistance and enable progress toward malaria elimination (Wei et al., 2021).

During blood-stage growth, *P. falciparum* internalizes hemoglobin in an endocytic process known as host cell cytosol uptake (HCCU) (Aikawa et al., 1966; Spielmann et al., 2020). Endocytosed hemoglobin is transported within vesicles to an acidic, lysosome-like parasite organelle termed food vacuole (FV), where hemoglobin is proteolytically digested to provide amino acids for synthesis of parasite proteins (Bakar et al., 2010; Jonscher et al., 2019; Milani et al., 2015). The digestion

of hemoglobin releases free heme, which is partly detoxified by crystallization into hemozoin (Hempelmann, 2007). The Fe(II) ion within the free heme catalyzes the production of reactive oxygen species (ROS) that cause the oxidation of unsaturated membrane phospholipids (PLs) (Bochkov et al., 2010; Das and Nanda, 1999; Fu et al., 2009). This process, termed lipid peroxidation, is toxic for cells as it causes drastic changes to membrane fluidity, rigidity, curvature, and permeability (Agmon et al., 2018; Borst et al., 2000; Runas and Malmstadt, 2015). Efficient repair of lipid-peroxidation damage is thus crucial for cell survival (Bochkov et al., 2010).

So far, no parasite enzyme that is involved in repair of lipid-peroxidation damage during blood-stage growth has been identified. However, RBCs contain a highly abundant lipid-peroxidation repair enzyme called peroxiredoxin 6 (PRDX6) (Gautier et al., 2018; Li et al., 2015). Mammalian PRDX6 is a conserved trifunctional enzyme with phospholipase A_2 (PLA_2), lysophosphatidylcholine acyl transferase (LPCAT), and cysteine-dependent peroxidase activities (Chowhan et al., 2020; Fisher, 2018; Fisher et al., 2016; Li et al., 2015; Wu et al., 2009). The PLA_2 function of PRDX6, which selectively cleaves oxidized fatty acid side chains and allows subsequent replacement with an unoxidized fatty acid through its LPCAT activity, is crucial for lipid-peroxidation-damage repair (Bochkov et al., 2010; Fisher, 2018; Fisher et al., 2016).

Here, we show that *P. falciparum* internalizes host RBC PRDX6 along with hemoglobin during blood-stage parasite development. We demonstrate that lipid peroxidation repair by PRDX6 is essential for parasite development and growth, identifying PRDX6 as a host-derived drug target against malaria parasites. Treatment of *P. falciparum* blood-stage cultures with a PLA_2 inhibitor, Darapladib, inhibits the PLA_2 activity of PRDX6 and blocks parasite growth. Moreover, co-treatment with Darapladib and ART synergistically reduces survival of ART-resistant *P. falciparum* strains in a ring-stage survival assay. The advantage of anti-malarial drugs that target host enzymes has been recently highlighted (Wei et al., 2021). The studies reported here identify PRDX6 as a potential host-based drug target and may provide a strategy to overcome ART resistance in *P. falciparum*.

RESULTS

P. falciparum imports host RBC PRDX6 along with hemoglobin

Given the abundance of PRDX6 in the RBC cytosol, we hypothesized that *P. falciparum* may internalize host PRDX6 along with hemoglobin during HCCU. To assess this, we selectively lysed the RBC membrane of *P. falciparum*-infected RBCs by saponin treatment and detected PRDX6 in purified parasites. Soluble protein lysate derived from saponin-liberated *P. falciparum* trophozoites was analyzed by mass spectrometry to identify internalized host RBC proteins. PRDX6 was one of 97 host RBC proteins that were detected with a high degree of confidence (>3 peptide-spectrum matches, PSM) in each of 15 independent experiments (Figure S1A; Table S3). The presence of PRDX6 in saponin-treated parasite fractions was also examined by western blotting using an anti-PRDX6 mouse monoclonal antibody. PRDX6 was detected in lysates of both intact *P. falciparum*-infected RBCs as well as saponin-treated parasite fractions (Figure S1B). At the same time, hemoglobin was detected only in intact parasite-infected RBCs and not in saponin-treated parasite fractions, confirming complete lysis of the RBC membrane and loss of the RBC cytosolic fraction (Figure S1B). Localization of human PRDX6 within the parasite in *P. falciparum*-infected RBCs was also confirmed by immunofluorescence microscopy. PRDX6 was evenly distributed in the cytosol of uninfected RBCs (Figure 1A). In contrast, multiple PRDX6-containing vesicles were detected adjacent to the parasite FV in *P. falciparum*-infected RBCs, suggesting endocytic uptake of PRDX6 by the parasite (Figure 1A). Three-dimensional quantification of the fluorescence signal demonstrated that PRDX6 levels were elevated within the parasite relative to the RBC cytosol in ring and trophozoite stages (Figure S1C). The internalization of PRDX6 by the parasite was further confirmed by immuno-electron microscopy (EM). As expected, uninfected RBCs showed uniform cytosolic staining of PRDX6 (Figure 1B), whereas in infected RBCs, PRDX6 was localized in electron-dense, hemoglobin-containing vesicular structures (Figures 1C–1F). PRDX6-containing vesicles were found at the inner surface of the parasite plasma membrane in structures that resembled cytostomes (Figures 1C–1E, black arrows), adjacent to the FV (Figures 1C–1E, white arrows) and in the parasite cytosol (Figure 1F, striped gray arrow). Taken together, these images demonstrate that host PRDX6 is internalized by *P. falciparum*. Furthermore, the data suggest that PRDX6 is internalized by endocytosis during HCCU and subsequently transported in hemoglobin-containing vesicles (HCVs) to the FV. PRDX6 was not detected inside the FV lumen, suggesting that it may be cleaved after delivery to the FV, which contains proteases involved in hemoglobin degradation (Francis et al., 1997).

The PLA_2 inhibitor Darapladib inhibits PRDX6 and blocks blood-stage growth by impairment of lipid-peroxidation repair

To investigate the role of PRDX6 during blood-stage growth, inhibitors of structurally and functionally related PLA_2 enzymes were screened for binding to the PLA_2 active site of PRDX6 by activity-based protein profiling (ABPP) using recombinant human PRDX6 (Figures S2A and S2B) and the fluorescently tagged probe TAMRA-FP that covalently labels the serine in the PLA_2 active site of PRDX6 (Figures 2A and S2C) (Cravatt et al., 2008). Inhibitors that bind the PLA_2 active site of PRDX6 compete with TAMRA-FP and reduce the fluorescent labeling of PRDX6. A range of PLA_2 inhibitors were tested for binding using ABPP (Figures 2A and S2C). While the inhibitors ATK, MAFP, and Darapladib bound PRDX6, Varespladib and P11 failed to bind. The different PLA_2 inhibitors were also tested *in vitro* for their ability to block *P. falciparum* blood-stage growth and progression from rings to schizonts. Synchronous *P. falciparum* 3D7 cultures were treated at the ring stage, and effects on ring-to-schizont development (“progression”) and multiplication following completion of a full blood-stage cycle (“growth”) were assessed by flow cytometry using the DNA intercalating fluorescent dye SYBR Green I (Figure 2B). Notably, inhibitors that bound PRDX6 (ATK, MAFP, and Darapladib) blocked parasite

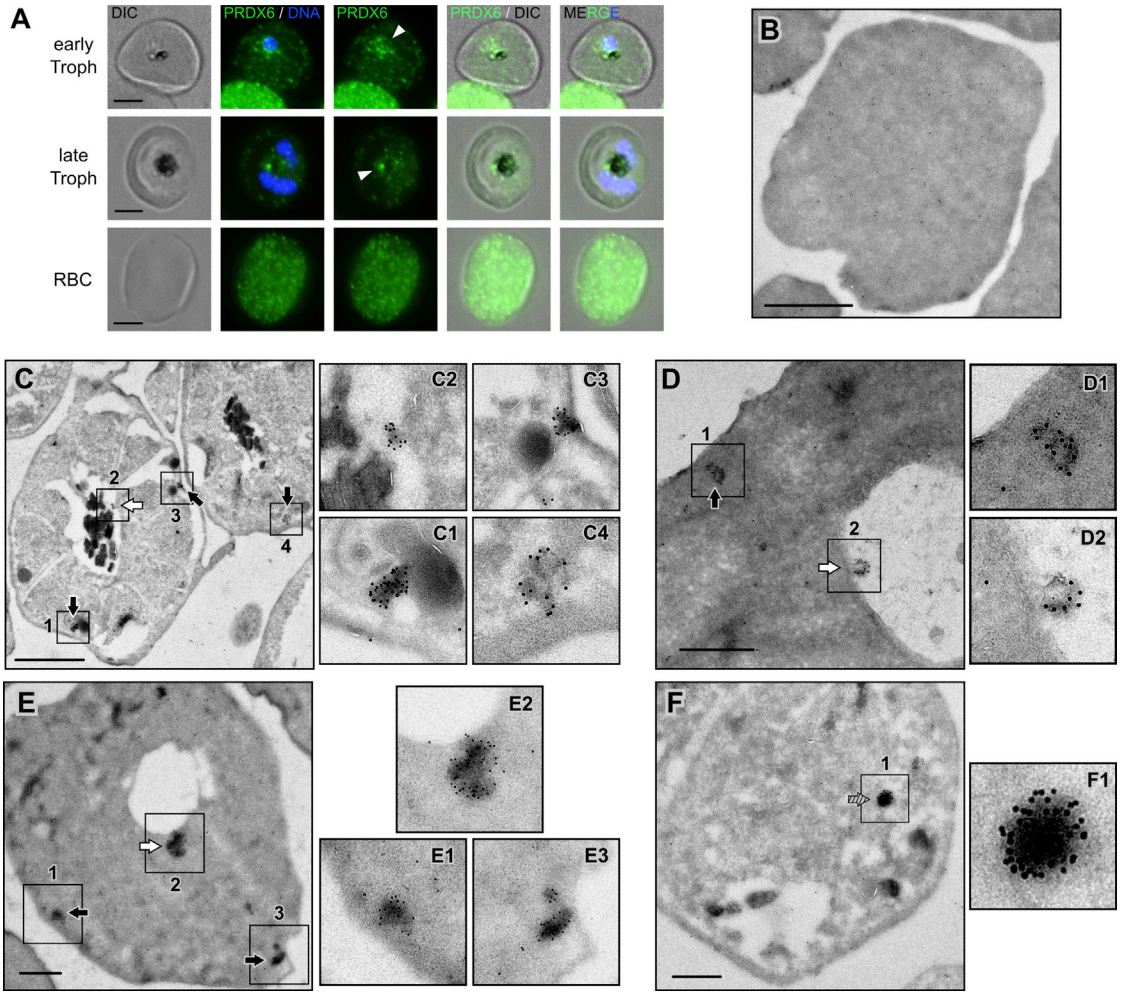

Figure 1. Human PRDX6 is internalized by *P. falciparum* along with hemoglobin during HCCU

(A) Immunofluorescence microscopy shows even cytosolic staining of PRDX6 in uninfected RBCs. In early and late trophozoites, multiple PRDX6 foci (white arrowheads) were observed adjacent to the parasite FV. DNA, Hoechst 33342 (nuclei). Scale bars, 5 μm. Representative images from three independent experiments are shown. See also Figures S1C and S1D.

(B–F) Immuno-transmission electron microscopy (TEM) using monoclonal mouse anti-PRDX6 antibody.

(B) Uninfected RBCs showing even cytosolic staining for PRDX6.

(C–F) *P. falciparum*-infected RBCs show co-localization of PRDX6 and hemoglobin in vesicles at the inner surface of the parasite plasma membrane in structures that resemble cytostomes (black arrows), at the FV (white arrows), or within the parasite cytosol (striped gray arrow). Scale bars, 500 nm. Representative images from three independent experiments are shown.

progression and growth, whereas inhibitors that did not bind PRDX6 (P11 and Varespladib) had no effect. All effective inhibitors arrested parasite development at the trophozoite stage (Figure 2C). Darapladib had the lowest half-maximal inhibitory concentration (IC_{50}) for parasite progression (0.56 μM) and growth (0.76 μM) (Figure 2B; Table S1) and was selected for further studies. As expected, Darapladib inhibited the PLA_2 activity of PRDX6 in a PLA_2 activity assay (Figure 2D).

To confirm that Darapladib specifically targets host PRDX6 to block blood-stage parasite development, we exploited *P. yoelii*-infected RBCs from transgenic *prdx6*$^{-/-}$ mice. We employed the *P. yoelii* YM lethal strain, which readily invades mature RBCs similar to *P. falciparum* (Otsuki et al., 2009). Immunofluorescence assays confirmed that PRDX6 is internalized by *P. yoelii* blood stages and is located in vesicles within the parasite (Figure S1D), as was observed earlier for *P. falciparum* (Figure 1). The sequence of PRDX6 is highly conserved among mammalian species with 93% similarity between mouse and human PRDX6 (Leyens et al., 2003). Transgenic mice that are null for PRDX6 are viable, possibly because they compensate for loss of PRDX6 by increased expression of other antioxidant enzymes and higher glutathione levels (Feinstein, 2019; Melhem et al., 2017). Indeed, RBCs from *prdx6*$^{-/-}$ mice had significantly higher levels of PRDX2 compared with RBCs from wild-type (WT) mice (Figure S3). It was, therefore, not surprising to find that growth of *P. yoelii* YM was similar in WT and *prdx6*$^{-/-}$ mice (Figure 2E). This

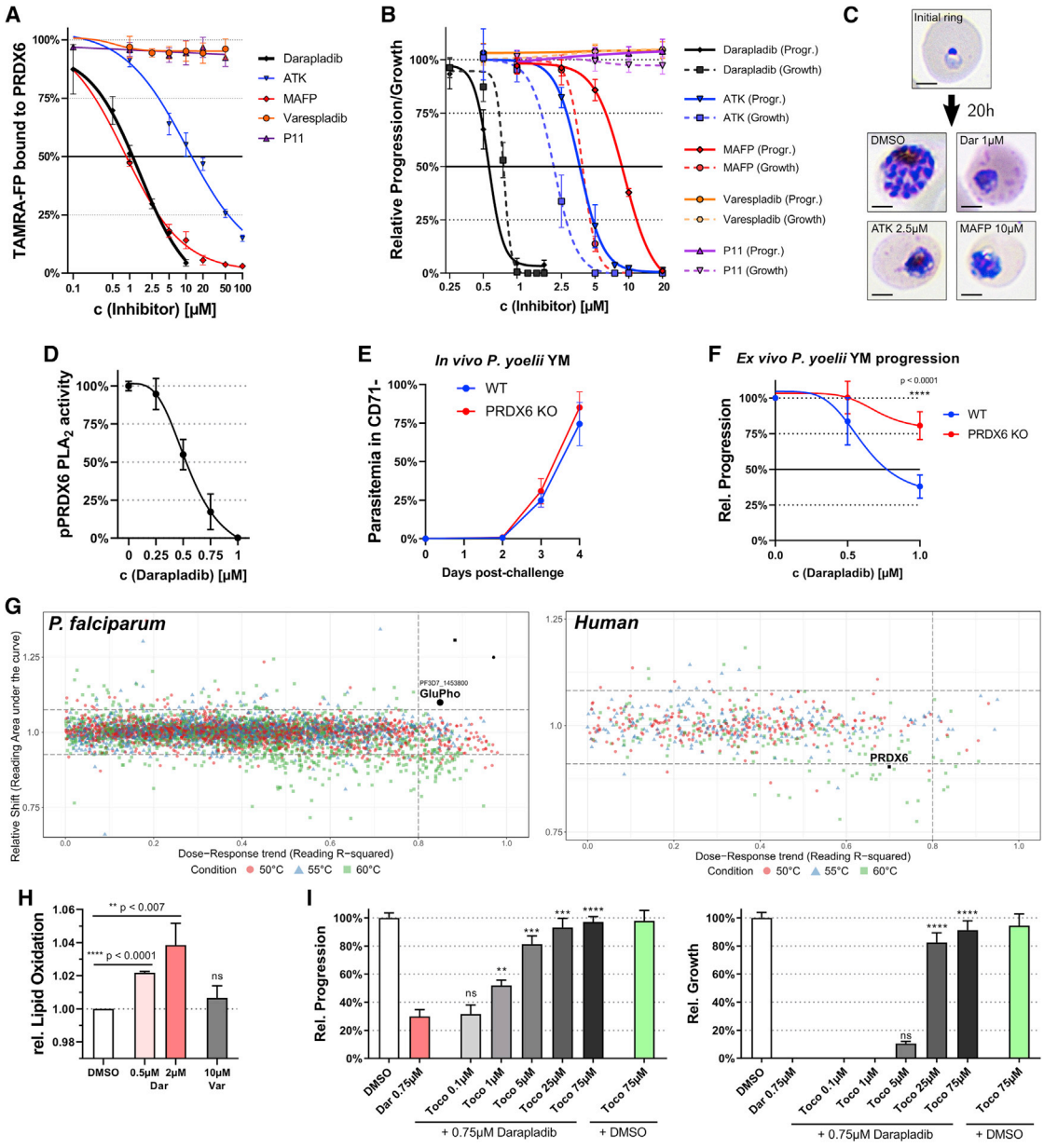

Figure 2. Darapladib selectively inhibits PRDX6 and blocks *P. falciparum* growth by impeding lipid-peroxidation repair

(A) Binding of TAMRA-FP with recombinant PRDX6 in the presence of different PLA_2 inhibitors in activity-based protein profiling (ABPP) assays. Reduced labeling of PRDX6 by TAMRA-FP identifies PLA_2 inhibitors that bind PRDX6. See also Figure S2C.

(B) Inhibition of *P. falciparum* ring-to-schizont progression and blood-stage growth with PLA_2 inhibitors. Parasites were treated at ring stage, and growth to schizont stage in the same cycle ("progression") or to next-generation rings ("growth") was scored by flow cytometry using DNA intercalating fluorescent dye SYBR Green I. See also Table S1.

(C) Representative light microscopy images of control and treated *P. falciparum* blood stages showing arrest at the trophozoite stage following treatment with different inhibitors at ring stage. Scale bars, 5 μm.

(D) Radioactive PLA_2 activity assay using phosphorylated recombinant human PRDX6 in presence or absence of Darapladib. Darapladib inhibits PLA_2 activity of PRDX6 with IC50 of ≈0.5 μM.

(E) Flow-cytometric measurement of *in vivo* growth curves of *P. yoelii* YM in C57BL/6 WT and *prdx6*$^{-/-}$ mice. *In vivo* infection was performed two times independently with five mice per group.

(F) *Ex vivo* ring-to-schizont progression of *P. yoelii* YM in CD71^{-} mature RBCs from WT and *prdx6*$^{-/-}$ mice in the presence and absence of Darapladib. Darapladib inhibits *P. yoelii* YM progression from ring-to-schizont stage in WT RBCs at a concentration of 1 μM but not in *prdx6*$^{-/-}$ mouse RBCs.

(G) ITDR-CETSA analysis of protein target engagement by Darapladib (0–100 μM) in trophozoite lysate. Distribution of protein stabilizations, under 50°C (red circle), 55°C (blue triangle), and 60°C (green squares) thermal challenges, is plotted as a function of R^2 value (goodness of curve fit) against ΔAUC (area under the curve of heat-challenged sample normalized against non-denaturing 37°C control) for all proteins detected in the assay. Two and half times of median absolute

(legend continued on next page)

allowed us to assess the effect of Darapladib on *ex vivo* progression of *P. yoelii* YM from ring-to-schizont stages in RBCs from WT and *prdx6*$^{-/-}$ mice (Figure 2F). Darapladib blocked *ex vivo* progression of the *P. yoelii* YM strain in WT mouse RBCs but had no effect on progression in RBCs from *prdx6*$^{-/-}$ mice up to a concentration of 1 μM, confirming that it specifically targets PRDX6 (Figure 2F).

To identify possible off-targets of Darapladib in *P. falciparum*-infected RBCs, we carried out a mass-spectrometry-based isothermal dose-response cellular thermal shift assay (ITDR-MS-CETSA) (Figures 2G and S2D) (Dziekan et al., 2019, 2020). Parasite lysate was exposed to varying concentrations of Darapladib and heat challenged to denature unstable protein subsets. After centrifugation, the remaining soluble protein fraction was analyzed by quantitative mass spectrometry. Among 1,801 parasite proteins detected in both biological replicates, drug-dose-dependent stabilization was observed for only one essential *P. falciparum* enzyme, glucose-6-phosphate dehydrogenase-6-phosphogluconolactonase (*Pf*GluPho) (Figure S2D). Using both recombinant *Pf*GluPho as well as parasite lysate, we found that Darapladib did not inhibit the essential glucose-6-phosphate dehydrogenase (G6PD) activity of *Pf*GluPho in orthogonal enzymatic assays (Figures S2E and S2F). *Pf*GluPho was thus ruled out as an off-target of Darapladib.

In a corresponding analysis carried out for the human proteome (n = 280), no drug-induced protein stabilizations were identified. Interestingly, PRDX6 was found to exhibit significant (>2.5 median absolute deviation [MAD] of ΔAUC) dose-dependent destabilization under Darapladib treatment at 60°C. Protein destabilization induced by ligand binding is a non-canonical, but well-established, phenomenon (Botelho et al., 2009; Cimmperman et al., 2008; Dai et al., 2014; Lim et al., 2018). To cross-validate the observed destabilization of PRDX6 by Darapladib, we employed differential scanning fluorimetry (DSF). In a corresponding DSF experiment, Darapladib caused a reproducible decrease in melting temperature of recombinant PRDX6, in agreement with CETSA results (Figure S2G).

PRDX6 is a lipid-peroxidation repair enzyme involved in protection of cells from oxidative damage. The fluorescent lipid-peroxidation sensor BODIPY$^{581/591}$ C11 was used to assess whether treatment of *P. falciparum*-infected RBCs with Darapladib resulted in increased lipid-peroxidation damage (Figure 2H). As expected, Darapladib treatment increased lipid-peroxidation damage in *P. falciparum* blood stages in a dose-dependent manner (Figure 2H). Increased lipid-peroxidation damage was also confirmed independently by measurement of malondialdehyde (MDA) (Figure S4A). To further confirm the involvement of PRDX6 in lipid-peroxidation repair, we co-treated parasites with Darapladib and the lipophilic antioxidant α-tocopherol (vitamin E), which prevents lipid peroxidation by scavenging radicals (Niki, 2014). Co-treatment with α-tocopherol rendered Darapladib ineffective and restored parasite progression and growth in a dose-dependent manner (Figure 2I). These observations further demonstrate that host PRDX6 is essential for repair of lipid-peroxidation damage during *P. falciparum* blood-stage development.

Inhibition of PRDX6 blocks vesicular transport of hemoglobin to FV

The localization of PRDX6 within HCVs and inhibition of progression at trophozoite stage suggested that PRDX6 may play a role in HCCU and hemoglobin catabolism. We, therefore, tested the impact of Darapladib treatment on hemoglobin transport to the FV. For this, we co-treated parasites with Darapladib and the cysteine protease inhibitor E64 that blocks proteolytic digestion of hemoglobin leading to bloating of the FV (Lazarus et al., 2008). As expected, E64 treatment led to an enlarged FV due to accumulation of undigested hemoglobin, as observed by light microscopy (Figures 3A and 3B) and transmission EM (Figure 3C). In contrast, treatment with Darapladib, either alone or with E64, prevented bloating of the FV and resulted in parasites with a shrunken FV that contained little to no hemozoin, suggesting that Darapladib acts upstream of hemoglobin digestion in the FV (Figures 3A and 3C). Moreover, multiple HCVs were observed in the parasite cytosol upon treatment with Darapladib (Figure 3C). Taken together, these observations suggest that PRDX6 is not involved in HCCU and HCV formation but is essential for active transport of HCVs to the FV.

To confirm that PRDX6 inhibition leads to disruption of delivery of host cell cytosol to the FV, we preloaded RBCs with pH-dependent LysoSensor Blue/Yellow that emits blue fluorescence at neutral pH, as found in the cytosol, and yellow fluorescence at acidic pH, as found in the FV. RBCs preloaded with LysoSensor Blue/Yellow were infected with *P. falciparum*, treated at ring stage, and allowed to develop into trophozoites. Control parasites successfully internalized host cell cytosol and exhibited a bright yellow signal in the FV (Figures 3D–3F). Inhibition of PRDX6 with Darapladib reduced yellow fluorescence signal intensity, and parasites appeared shrunken and pyknotic without visible hemozoin. Furthermore, treatment of *P. falciparum* rings with Darapladib significantly decreased the size of hemozoin crystals (Figure S4B). Taken together, these observations show that PRDX6 is essential for the transport of hemoglobin to the FV.

Co-treatment of ART-resistant parasites with ART and Darapladib synergistically reduces parasite survival

Resistance against the frontline anti-malarial drug ART is a major threat for malaria control and elimination efforts. Parasites attain

deviation (MAD) of ΔAUC in each dataset and R^2 = 0.8 cut offs are indicated. Hits surpassing selection criteria, as well as PRDX6, are plotted in black. Thermal stability profiles for these hits are provided in Figure S2D. GluPho, glucose-6-phosphate dehydrogenase-6-phosphogluconolactonase. Data from two independent experiments. See also Figure S2E.

(H) Quantification of lipid-peroxidation damage using flow-cytometric measurement of the fluorescent lipid-peroxidation sensor BODIPY$^{581/591}$ C11 following treatment of parasites with Darapladib (Dar) or Varespladib (Var) for 2 h at trophozoite stage. See also Figure S4A.

(I) Ring-to-schizont progression and full-cycle growth curves following treatment with Dar and α-tocopherol (Toco) co-treatment. Parasites were treated at ring stage. ns, $p > 0.05$; * $p \leq 0.05$; ** $p \leq 0.01$; *** $p \leq 0.001$; **** $p \leq 0.0001$

Data in (A)–(C), (F), (H), and (I) are means ± SD of three independent experiments, unpaired t test.

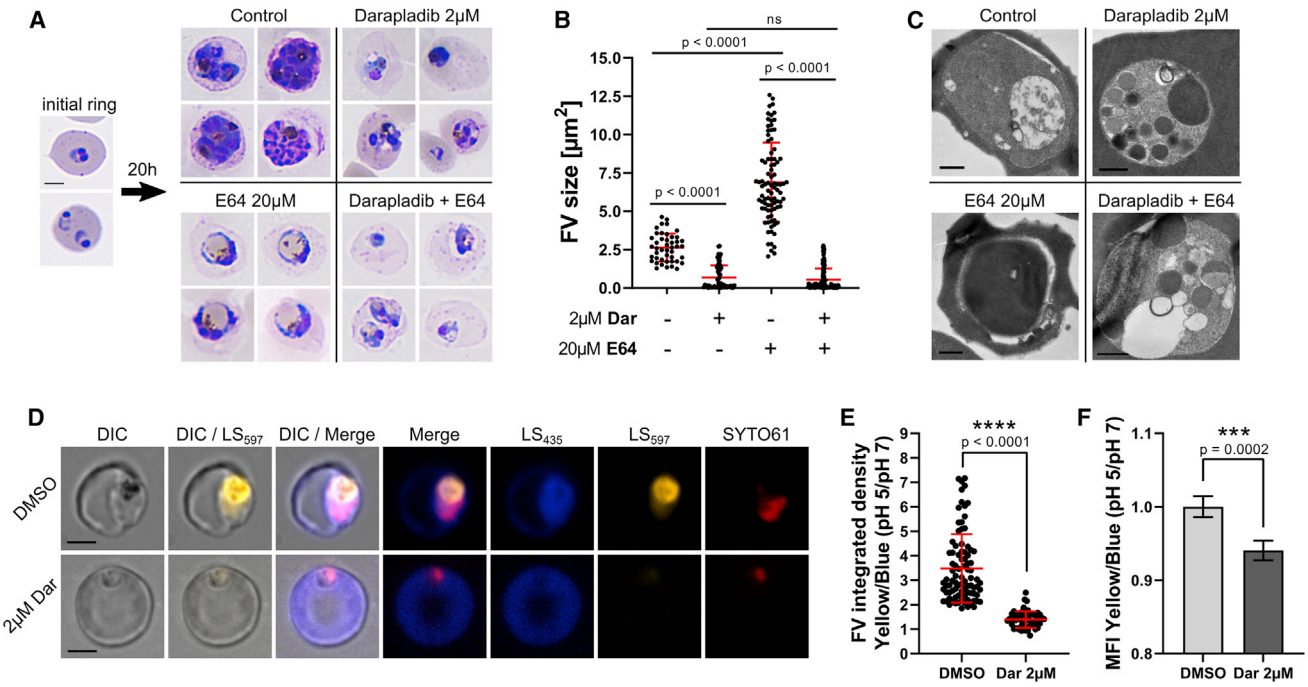

Figure 3. Inhibition of PRDX6 blocks vesicular transport of hemoglobin-containing vesicles (HCVs) to the FV

(A) Light microscopy of *P. falciparum* blood-stage cultures treated at the ring stage with Dar, E64, or Dar + E64 and incubated for 20 h. Treatment of *P. falciparum* rings with E64 resulted in bloating of the FV with undigested hemoglobin. In contrast, treatment with either Dar alone or with E64 prevented E64-mediated bloating of the FV, indicating a role of PRDX6 upstream of hemoglobin digestion. Scale bars, 5 μm. Representative images from three independent experiments are shown.

(B) Quantification of FV size observed in (A).

(C) TEM of *P. falciparum* blood-stage cultures from (A). Dar arrested transport of HCVs within the parasite cytosol. Scale bars, 500 nm.

(D) Fluorescence microscopy. Use of pH-sensitive fluorescent probe to observe HCCU in *P. falciparum* blood stages following treatment with Dar. RBCs were preloaded with pH-sensitive LysoSensor Blue/Yellow, infected with *P. falciparum*, treated with Dar at the ring stage, and imaged at the trophozoite stage. Dar treatment prevented transport of RBC cytosol (neutral pH, blue) to the FV (acidic, yellow). Scale bars, 5 μm. DIC, differential interference contrast; LS_{435}, LysoSensor at neutral pH; LS_{597}, LysoSensor at acidic pH; SYTO61, DNA (nuclei).

(E) Quantification of Yellow/Blue signal ratio within the FV observed by fluorescence microscopy in (D).

(F) Flow-cytometric measurement of Yellow/Blue signal in *P. falciparum*-infected RBCs treated with Dar as described in (D).

(A–F) Representative images or means ± SD from three independent experiments, unpaired t tests.

ART resistance through reduced hemoglobin uptake and digestion, which lowers oxidative-stress levels and precludes activation of ART (Birnbaum et al., 2020; Xie et al., 2020). As inhibition of PRDX6 by Darapladib raises oxidative-stress levels, we investigated whether co-treatment with Darapladib and ART could restore ART susceptibility in ring-stage survival assays (RSAs) (Witkowski et al., 2013). RSAs with *P. falciparum* ring stages co-treated with Darapladib and Dihydroartemisinin (DHA), one of the ART derivatives used as first-line anti-malarials, showed synergistically reduced survival of NF54 $Kelch13^{C580Y}$ with complete reversal of ART resistance at 1 μM Darapladib (Figure 4A; Table S2). The ART-resistant field isolate from Cambodia, *P. falciparum* 3815 (Ariey et al., 2014), was also susceptible to co-treatment with Darapladib and DHA in the RSA (Figure 4A; Table S2). Both these parasites have the $Kelch13^{C580Y}$ mutation but in different genetic backgrounds. Survival of the highly resistant field isolate 3601 carrying the $Kelch13^{R539T}$ mutation also decreased following Darapladib co-treatment with ART, although the reduction was less compared with the NF54 $Kelch13^{C580Y}$ and 3815 strains (Figure 4A; Table S2). However, Darapladib effectively blocked blood-stage growth of all tested strains, with both $Kelch13^{R539T}$ and $Kelch13^{C580Y}$ mutations following continuous treatment during the complete blood-stage cycle (Figure 4B). Summed up, Darapladib could thus both reduce survival of ART-resistant parasites when combined with ART as well as independently block parasite growth of ART-resistant *P. falciparum* strains.

DISCUSSION

The import and proteolytic degradation of hemoglobin during *P. falciparum* blood-stage growth creates significant oxidative stress that can cause oxidative damage to both host and parasite lipid membranes. Interestingly, *P. falciparum* has been shown to internalize host antioxidant enzymes such as catalase, superoxide dismutase, and PRDX2 by unknown mechanisms during blood-stage infection (Foth et al., 2011; Koncarevic et al., 2009). However, these enzymes exclusively detoxify small free ROS and are not involved in lipid-peroxidation repair. Mechanisms for the management and repair of lipid-peroxidation

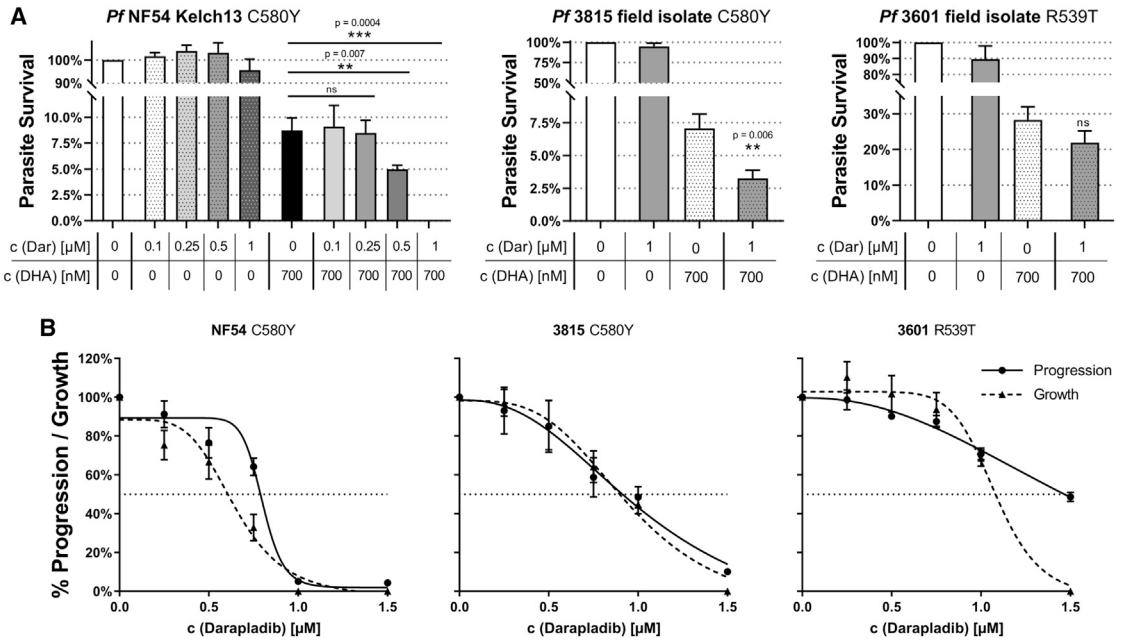

Figure 4. Co-treatment of ART-resistant parasites with artemisinin and Dar synergistically reduces parasite survival

(A) Ring-stage survival assays with Dar and Dihydroartemisinin (DHA) against ART-resistant *P. falciparum* strains. For detailed data regarding synergism, see Table S2.

(B) Growth/progression assay with continuous Dar treatment against ART-resistant *P. falciparum* strains. Data in (A) and (B) are means ± SD of three independent experiments, unpaired t tests.

damage during *P. falciparum* blood-stage growth are unclear, and no lipid-peroxidation repair enzymes have been identified in the parasite proteome (Flammersfeld et al., 2018; Fu et al., 2009). Here, we demonstrate that *P. falciparum* imports the host lipid-peroxidation repair enzyme PRDX6 during blood stage, allowing it to repair lipid-peroxidation damage. Moreover, we show that PRDX6 also plays an important role in the transport of HCVs to the FV.

HCCU is a key mechanism for the import of hemoglobin during blood-stage growth of malaria parasites. Research on HCCU has so far focused on uptake of hemoglobin but has neglected the potential import and role of other cytosolic RBC proteins. Our study shows that a host lipid-peroxidation repair enzyme, PRDX6, is internalized along with hemoglobin during HCCU. Early cytostomes and HCVs predominantly contain host cytosolic proteins. Thus, it is not surprising that antioxidant protection in these vesicles might primarily be facilitated by host cytosolic antioxidant enzymes. The observation that cytostomes and HCVs have higher concentrations of hemoglobin and PRDX6 than the RBC cytosol suggests protein uptake or enrichment mechanisms, which remain to be identified.

Based on our observations, we propose a model where PRDX6 is essential for lipid-peroxidation repair in nascent HCVs. Inhibition of PRDX6 leads to increase in lipid-peroxidation damage in HCVs due to lack of lipid repair, which appears to disrupt active transport of HCVs towards the FV. As a result, HCVs accumulate in trophozoite stages, as observed by EM of Darapladib-treated parasites. The mechanistic understanding of active transport of HCVs in *Plasmodium spp*. is unfortunately limited. In mammalian cells, vesicular transport is facilitated by actin-myosin motor proteins (Lee Sweeney and Holzbaur, 2018). Myosin binds to myosin receptors on the vesicle surface to anchor the motor and enable movement. Elevated lipid-peroxidation damage may disturb the localization or functioning of such receptors in the HCV membrane, disrupting normal attachment of HCVs to their respective motor proteins and leading to disruption of active transport. This notion is supported by several studies that implicate actin in HCV transport (Lazarus et al., 2008; Smythe et al., 2008). Conditional inactivation of the parasite protein *Pf*VPS45 causes a similar phenotype of arrested HCVs in the parasite cytosol, suggesting a functional role for *Pf*VPS45 in vesicular transport to the FV (Jonscher et al., 2019). In the liver stage of malaria parasites, inhibition of host glutathione peroxidase 4 (GPx4) has been shown to increase lipid-peroxidation damage and inhibit liver-stage parasite growth (Kain et al., 2020). PRDX6 is also expressed in hepatocytes and could mediate lipid-peroxidation-damage repair (Eismann et al., 2009; Fisher, 2018). It is thus possible that PRDX6 may also play a role in parasite growth in the liver stage.

Darapladib was originally developed as a selective inhibitor of extracellular lipoprotein-associated PLA_2 (Lp-PLA_2) (Blackie et al., 2003). However, Lp-PLA_2 is absent in RBCs and is also not internalized by *P. falciparum*-infected RBCs from blood serum (Gautier et al., 2018; Tougan et al., 2020; Zhou et al., 2011). Darapladib was shown to bind PRDX6 using ABPP and blocks the PLA_2 activity of PRDX6. The on-target specificity of Darapladib was demonstrated using RBCs from *prdx6*$^{-/-}$ mice that lack PRDX6. In the absence of PRDX6 in RBCs from

prdx6$^{-/-}$ mice, Darapladib loses its inhibitory effect on the progression of *P. yoelii* from rings to schizonts. The observation that Darapladib inhibits blood-stage progression of both *P. falciparum* and *P. yoelii* suggests a common mechanism for lipid-peroxidation-damage repair that is essential for parasite survival across different *Plasmodium* species. The specificity of Darapladib for PRDX6 was furthermore validated using ITDR-CETSA, which demonstrated that no other host or parasite protein is targeted by Darapladib. However, due to the relatively high IC_{50} of Darapladib for the inhibition of blood-stage growth ($\approx$0.5 μM), Darapladib itself is not suitable for use as an anti-malarial drug candidate. Also, due to the low bioavailability of Darapladib, inhibition of PRDX6 by Darapladib cannot be tested in a clinical *in vivo* malaria model (Dave et al., 2014). Since no high-affinity inhibitor of PRDX6 is known, improved inhibitors with a higher affinity to PRDX6 need to be identified and could serve as promising anti-malarial drug candidates.

Resistance to ART, one of the major threats to malaria-control efforts, which arose in *P. falciparum* strains in Southeast Asia, has now been identified on the African continent (Balikagala et al., 2021; Uwimana et al., 2021). Strategies to combat ART resistance are urgently needed. We found that co-treatment with ART and Darapladib synergistically reduced survival of ART-resistant parasites. PRDX6 inhibitors could thus play a pivotal role in restoring the efficacy of ART against ART-resistant strains. In addition, a PRDX6 inhibitor will independently block growth of *P. falciparum* blood stages by inhibiting transport of hemoglobin to the FV. An ART-based combination therapy involving ART together with a PRDX6-targeting partner drug would be effective in two ways: firstly, it could help to synergistically reduce ART-resistant parasite survival during the early ring stage, restoring ART susceptibility. Secondly, it would independently inhibit blood-stage growth of *P. falciparum* isolates including ART-resistant strains.

The identification of PRDX6, a host RBC enzyme that is essential for *P. falciparum* blood-stage growth, provides a host-based target for the development of therapeutic strategies for the treatment and control of malaria. Approaches that target host enzymes for development of anti-malarial drugs are attractive because parasites cannot mutate the target gene to attain resistance (Wei et al., 2021). Thus, inhibitors that target host enzymes such as PRDX6 are less likely to face the problem of drug resistance and could play a critical role in malaria-eradication efforts in the long term.

Limitations of the study

Here, we describe the role of host PRDX6 in the growth of *P. falciparum* blood stages and identify it as a potential drug target for malaria. As mature RBCs cannot be genetically modified, it is not possible to directly confirm the functional role of PRDX6 in *P. falciparum* blood-stage growth by genetic deletion. Although it is possible to genetically modify erythroid progenitor cells, which can then be differentiated into nucleated RBCs, this system is not suitable for our study because *P. falciparum* does not develop beyond the ring stage in these nucleated RBCs (Kanjee et al., 2017). The only feasible approach to directly investigate the role of PRDX6 was to use transgenic *prdx6*$^{-/-}$ mice and *P. yoelii*. However, possibly due to multiple compensatory changes in *prdx6*$^{-/-}$ mice, the growth of *P. yoelii* blood stages is not affected in these mice. Nevertheless, we could demonstrate that Darapladib treatment inhibits blood-stage growth of *P. yoelii* in normal mouse RBCs *in vitro* but has no effect on *P. yoelii* growth in *prdx6*$^{-/-}$ mouse RBCs, confirming that PRDX6 is indeed the target of Darapladib. Furthermore, a CETSA found no evidence that Darapladib has biologically significant interactions with off-targets in the human or *P. falciparum* proteomes. CETSA identifies proteins that undergo thermal stabilization (or destabilization) upon binding Darapladib but does not necessarily confirm inhibition of the enzymatic activity of the target enzyme. Fortunately, we could demonstrate that Darapladib both destabilizes PRDX6 and inhibits its PLA_2 activity. Due to the high IC_{50} of Darapladib for inhibition of PRDX6 activity as well as poor bioavailability, it is not possible to directly test Darpladib as a drug for malaria. It is necessary to identify Darapladib analogs or PLA_2 inhibitors with better IC_{50} for inhibition of PLA_2 activity as well as bioavailability characteristics that can be used as leads for the development of drugs against malaria. Such studies are currently underway. While we clearly demonstrate that Darapladib treatment blocks transport of PRDX6- and Hb-containing vesicles to the FV, the study does not identify the mechanism for uptake of PRDX6 by the parasite. This question merits separate investigation that is beyond the scope of this paper.

STAR★METHODS

Detailed methods are provided in the online version of this paper and include the following:

- KEY RESOURCES TABLE
- RESOURCE AVAILABILITY
  - Lead contact
  - Materials availability
  - Data and code availability
- EXPERIMENTAL MODEL AND SUBJECT DETAILS
  - *Plasmodium falciparum* parasites
  - Red blood cells
  - *In vivo* infection of mice with *P. yoelii*
- METHOD DETAILS
  - Lysis with saponin and sample preparation
  - SDS-PAGE and immunoblotting
  - Immunofluorescence microscopy
  - Transmission electron microscopy
  - EPON resin embedding
  - Recombinant expression of human PRDX6
  - Activity-based protein profiling of PRDX6
  - PRDX6 phosphorylation and PLA_2 activity assay
  - Parasite progression and growth assay
  - Infection of mice with *P. yoelii*
  - *Ex vivo P. yoelii* YM progression assay
  - Mass spectrometry detection
  - MS-IDTR-CETSA and analysis
  - Differential scanning fluorimetry of PRDX6
  - Recombinant expression of *P. falciparum* GluPho
  - Glucose-6-phosphate dehydrogenase activity assay
  - Lipid peroxidation measurement with $BODIPY^{581/591}$ C11

SUPPLEMENTAL INFORMATION

Supplemental information can be found online at https://doi.org/10.1016/j.celrep.2022.110923.

ACKNOWLEDGMENTS

We thank Gordon Langsley for fruitful discussions and critical inputs. We also thank the electron microscopy Ultrastructural BioImaging (UBI) platform, Institut Pasteur, Paris, for providing ready access to the electron microscopy facility. The authors are grateful to the Central Animal Facility of Institut Pasteur for providing support with animal importation, care, housing, and breeding. We thank the Image Analysis Hub (IAH), Institut Pasteur, Paris, for their help with image analysis. M.P.W. was part of the Pasteur - Paris University (PPU) International PhD Program and European Union's Horizon 2020 research and innovation program under the Marie Sklodowska-Curie grant agreement no. 665807. This work was funded by the following grants: Fondation pour la Recherche Médicale grant (FDT202001010791) to M.P.W.; Agence Nationale de la Recherche grant (ANR-17-CE15-0010) to C.E.C.; Pasteur Innov grant from Institut Pasteur to C.E.C.; Laboratoire d'Excellence (LabEx) "French Parasitology Alliance For Health Care" (ANR-11-LABX-0024-PARAFRAP) to C.E.C. and D.M.; Laboratoire d'Excellence "Integrative Biology of Emerging Infectious Diseases" (grant no. ANR-10-LABX-62-IBEID) to P.F.; NTU Presidential Postdoctoral Fellowship grant (NTU/PPF/2019) to J.M.D.; Singaporean Ministry of Education grant (MOE-T2EP30120-0015) to J.M.D. and Z.B.; and LOEWE Center DRUID (Projects B3) within the Hessian Excellence Program to I.B.

AUTHOR CONTRIBUTIONS

Conceptualization, M.P.W. and C.E.C.; methodology, M.P.W., L.T., and C.E.C.; investigation, M.P.W., P.F., O.G., J.M.D., and I.B.; funding acquisition, C.E.C. and M.P.W.; project administration, C.E.C.; supervision, C.E.C.; resources, D.M., J.-C.B., R.A., C.H., S.R., Z.B., A.B.F., and S.I.F.; writing, M.P.W. and C.E.C.

DECLARATION OF INTERESTS

A patent application has been filed by Institut Pasteur based on the results of this publication with M.P.W., C.E.C., L.T., O.G., C.H., P.F., and R.H. as inventors. A.B.F. and S.I.F. are shareholders in Peroxitech, Inc., a USA company that is developing a peptide-based PRDX6 inhibitor as a therapeutic agent.

Received: November 29, 2021
Revised: March 30, 2022
Accepted: May 17, 2022
Published: June 14, 2022

REFERENCES

Agmon, E., Solon, J., Bassereau, P., and Stockwell, B.R. (2018). Modeling the effects of lipid peroxidation during ferroptosis on membrane properties. Sci. Rep. *8*, 5155. https://doi.org/10.1038/s41598-018-23408-0.

Aikawa, M., Huff, C.G., and Sprinz, H. (1966). Comparative feeding mechanisms of avian and primate malarial parasites. Mil. Med. *131*, 969–983. https://doi.org/10.1093/milmed/131.suppl_9.969.

Ariey, F., Witkowski, B., Amaratunga, C., Beghain, J., Langlois, A.C., Khim, N., Kim, S., Duru, V., Bouchier, C., Ma, L., et al. (2014). A molecular marker of artemisinin-resistant Plasmodium falciparum malaria. Nature *505*, 50–55. https://doi.org/10.1038/nature12876.

Bakar, N.A., Klonis, N., Hanssen, E., Chan, C., and Tilley, L. (2010). Digestive-vacuole genesis and endocytic processes in the early intraerythrocytic stages of Plasmodium falciparum. J. Cell Sci. *123*, 441–450. https://doi.org/10.1242/jcs.061499.

Balikagala, B., Fukuda, N., Ikeda, M., Katuro, O.T., Tachibana, S.-I., Yamauchi, M., Opio, W., Emoto, S., Anywar, D.A., Kimura, E., et al. (2021). Evidence of artemisinin-resistant malaria in Africa. N. Engl. J. Med. *385*, 1163–1171. https://doi.org/10.1056/nejmoa2101746.

Birnbaum, J., Scharf, S., Schmidt, S., Jonscher, E., Hoeijmakers, W.A.M., Flemming, S., Toenhake, C.G., Schmitt, M., Sabitzki, R., Bergmann, B., et al. (2020). A Kelch13-defined endocytosis pathway mediates artemisinin resistance in malaria parasites. Science *367*, 51–59. https://doi.org/10.1126/science.aax4735.

Blackie, J.A., Bloomer, J.C., Brown, M.J.B., Cheng, H.Y., Hammond, B., Hickey, D.M.B., Ife, R.J., Leach, C.A., Lewis, V.A., Macphee, C.H., et al. (2003). The identification of clinical candidate SB-480848: a potent inhibitor of lipoprotein-associated phospholipase A2. Bioorg. Med. Chem. Lett *13*, 1067–1070. https://doi.org/10.1016/s0960-894x(03)00058-1.

Bochkov, V.N., Oskolkova, O.V., Birukov, K.G., Levonen, A.L., Binder, C.J., and Stöckl, J. (2010). Generation and biological activities of oxidized phospholipids. Antioxidants Redox Signal. *12*, 1009–1059. https://doi.org/10.1089/ars.2009.2597.

Borst, J.W., Visser, N.V., Kouptsova, O., and Visser, A.J.W.G. (2000). Oxidation of unsaturated phospholipids in membrane bilayer mixtures is accompanied by membrane fluidity changes. Biochim. Biophys. Acta Mol. Cell Biol. Lipids *1487*, 61–73. https://doi.org/10.1016/s1388-1981(00)00084-6.

Botelho, H.M., Koch, M., Fritz, G., and Gomes, C.M. (2009). Metal ions modulate the folding and stability of the tumor suppressor protein S100A2. FEBS J. *276*, 1776–1786. https://doi.org/10.1111/j.1742-4658.2009.06912.x.

Chowhan, R.K., Rahaman, H., and Singh, L.R. (2020). Structural basis of peroxidase catalytic cycle of human Prdx6. Sci. Rep. *10*, 17416. https://doi.org/10.1038/s41598-020-74052-6.

Cimmperman, P., Baranauskiene, L., Jachimovičiute, S., Jachno, J., Torresan, J., Michailoviene, V., Matuliene, J., Sereikaite, J., Bumelis, V., and Matulis, D. (2008). A quantitative model of thermal stabilization and destabilization of proteins by ligands. Biophys. J. *95*, 3222–3231. https://doi.org/10.1529/biophysj.108.134973.

Cravatt, B.F., Wright, A.T., and Kozarich, J.W. (2008). Activity-based protein profiling: from enzyme chemistry to proteomic chemistry. Annu. Rev. Biochem. *77*, 383–414. https://doi.org/10.1146/annurev.biochem.75.101304.124125.

Dai, R., Wilson, D.J., Geders, T.W., Aldrich, C.C., and Finzel, B.C. (2014). Inhibition of Mycobacterium tuberculosis transaminase BioA by aryl hydrazines and hydrazides. Chembiochem *15*, 575–586. https://doi.org/10.1002/cbic.201300748.

Das, B.S., and Nanda, N.K. (1999). Evidence for erythrocyte lipid peroxidation in acute falciparum malaria. Trans. R. Soc. Trop. Med. Hyg. *93*, 58–62. https://doi.org/10.1016/s0035-9203(99)90180-3.

Dave, M., Nash, M., Young, G.C., Ellens, H., Magee, M.H., Roberts, A.D., Taylor, M.A., Greenhill, R.W., and Boyle, G.W. (2014). Disposition and metabolism of Darapladib, a lipoprotein-associated phospholipase A2 inhibitor, in humans. Drug Metab. Dispos. *42*, 415–430. https://doi.org/10.1124/dmd.113.054486.

Dziekan, J.M., Wirjanata, G., Dai, L., Go, K.D., Yu, H., Lim, Y.T., Chen, L., Wang, L.C., Puspita, B., Prabhu, N., et al. (2020). Cellular thermal shift assay for the identification of drug–target interactions in the Plasmodium falciparum proteome. Nat. Protoc. *15*, 1881–1921. https://doi.org/10.1038/s41596-020-0310-z.

Dziekan, J.M., Yu, H., Chen, D., Dai, L., Wirjanata, G., Larsson, A., Prabhu, N., Sobota, R.M., Bozdech, Z., and Nordlund, P. (2019). Identifying purine nucleoside phosphorylase as the target of quinine using cellular thermal shift assay.

Sci. Transl. Med. *11*, eaau3174. https://doi.org/10.1126/scitranslmed.aau3174.

Eismann, T., Huber, N., Shin, T., Kuboki, S., Galloway, E., Wyder, M., Edwards, M.J., Greis, K.D., Shertzer, H.G., Fisher, A.B., and Lentsch, A.B. (2009). Peroxiredoxin-6 protects against mitochondrial dysfunction and liver injury during ischemia-reperfusion in mice. Am. J. Physiol. Gastrointest. Liver Physiol. *296*, G266–G274. https://doi.org/10.1152/ajpgi.90583.2008.

Feinstein, S.I. (2019). Mouse Models of Genetically Altered Peroxiredoxin 6. Antioxidants *8*, 77.

Fisher, A.B. (2018). The phospholipase A2 activity of peroxiredoxin 6 [S]. J. Lipid Res. *59*, 1132–1147. https://doi.org/10.1194/jlr.r082578.

Fisher, A.B., Dodia, C., Sorokina, E.M., Li, H., Zhou, S., Raabe, T., and Feinstein, S.I. (2016). A novel lysophosphatidylcholine acyl transferase activity is expressed by peroxiredoxin 6. J. Lipid Res. *57*, 587–596. https://doi.org/10.1194/jlr.m064758.

Flammersfeld, A., Lang, C., Flieger, A., and Pradel, G. (2018). Phospholipases during membrane dynamics in malaria parasites. Int. J. Med. Microbiol. *308*, 129–141. https://doi.org/10.1016/j.ijmm.2017.09.015.

Foth, B.J., Zhang, N., Chaal, B.K., Sze, S.K., Preiser, P.R., and Bozdech, Z. (2011). Quantitative time-course profiling of parasite and host cell proteins in the human malaria parasite Plasmodium falciparum. Mol. Cell. Proteomics *10*, M110.006411. https://doi.org/10.1074/mcp.m110.006411.

Francis, S.E., Sullivan, D.J., and Goldberg, a.D.E. (1997). Hemoglobin metabolism IN the malaria parasite *plasmodium falciparum*. Annu. Rev. Microbiol. *51*, 97–123. https://doi.org/10.1146/annurev.micro.51.1.97.

Fu, Y., Klonis, N., Suarna, C., Maghzal, G.J., Stocker, R., and Tilley, L. (2009). A phosphatidylcholine-BODIPY 581/591 conjugate allows mapping of oxidative stress in P. falciparum-infected erythrocytes. Cytom. Part A *75*, 390–404. https://doi.org/10.1002/cyto.a.20704.

Gautier, E.F., Leduc, M., Cochet, S., Bailly, K., Lacombe, C., Mohandas, N., Guillonneau, F., El Nemer, W., and Mayeux, P. (2018). Absolute proteome quantification of highly purified populations of circulating reticulocytes and mature erythrocytes. Blood Adv. *2*, 2646–2657. https://doi.org/10.1182/bloodadvances.2018023515.

Hempelmann, E. (2007). Hemozoin biocrystallization in Plasmodium falciparum and the antimalarial activity of crystallization inhibitors. Parasitol. Res. *100*, 671–676. https://doi.org/10.1007/s00436-006-0313-x.

Jonscher, E., Flemming, S., Schmitt, M., Sabitzki, R., Reichard, N., Birnbaum, J., Bergmann, B., Höhn, K., and Spielmann, T. (2019). PfVPS45 is required for host cell cytosol uptake by malaria blood stage parasites. Cell Host Microbe *25*, 166–173.e5. https://doi.org/10.1016/j.chom.2018.11.010.

Jortzik, E., Mailu, B.M., Preuss, J., Fischer, M., Bode, L., Rahlfs, S., and Becker, K. (2011). Glucose-6-phosphate dehydrogenase-6-phosphogluconolactonase: a unique bifunctional enzyme from Plasmodium falciparum. Biochem. J. *436*, 641–650. https://doi.org/10.1042/bj20110170.

Kain, H.S., Glennon, E.K.K., Vijayan, K., Arang, N., Douglass, A.N., Fortin, C.L., Zuck, M., Lewis, A.J., Whiteside, S.L., Dudgeon, D.R., et al. (2020). Liver stage malaria infection is controlled by host regulators of lipid peroxidation. Cell Death Differ. *27*, 44–54. https://doi.org/10.1038/s41418-019-0338-1.

Kanjee, U., Grüring, C., Chaand, M., Lin, K.M., Egan, E., Manzo, J., Jones, P.L., Yu, T., Barker, R., Weekes, M.P., and Duraisingh, M.T. (2017). CRISPR/Cas9 knockouts reveal genetic interaction between strain-transcendent erythrocyte determinants of Plasmodium falciparum invasion. Proc. Natl. Acad. Sci. U S A *114*, E9356–E9365. https://doi.org/10.1073/pnas.1711310114.

Katsumata, M., Gupta, C., and Goldman, A.S. (1986). A rapid assay for activity of phospholipase A2 using radioactive substrate. Anal. Biochem. *154*, 676–681. https://doi.org/10.1016/0003-2697(86)90046-1.

Koncarevic, S., Rohrbach, P., Deponte, M., Krohne, G., Prieto, J.H., Yates, J., Rahlfs, S., and Becker, K. (2009). The malarial parasite Plasmodium falciparum imports the human protein peroxiredoxin 2 for peroxide detoxification. Proc. Natl. Acad. Sci. U S A *106*, 13323–13328. https://doi.org/10.1073/pnas.0905387106.

Lazarus, M.D., Schneider, T.G., and Taraschi, T.F. (2008). A new model for hemoglobin ingestion and transport by the human malaria parasite Plasmodium falciparum. J. Cell Sci. *121*, 1937–1949. https://doi.org/10.1242/jcs.023150.

Lee Sweeney, H., and Holzbaur, E.L.F. (2018). Motor proteins. Cold Spring Harb. Perspect. Biol. *10*, a021931. https://doi.org/10.1101/cshperspect.a021931.

Leyens, G., Donnay, I., and Knoops, B. (2003). Cloning of bovine peroxiredoxins—gene expression in bovine tissues and amino acid sequence comparison with rat, mouse and primate peroxiredoxins. Comp. Biochem. Physiol. Part B Biochem. Mol. Biol. *136*, 943–955. https://doi.org/10.1016/s1096-4959(03)00290-2.

Li, H., Benipal, B., Zhou, S., Dodia, C., Chatterjee, S., Tao, J.Q., Sorokina, E.M., Raabe, T., Feinstein, S.I., and Fisher, A.B. (2015). Critical role of peroxiredoxin 6 in the repair of peroxidized cell membranes following oxidative stress. Free Radic. Biol. Med. *87*, 356–365. https://doi.org/10.1016/j.freeradbiomed.2015.06.009.

Lim, Y.T., Prabhu, N., Dai, L., Go, K.D., Chen, D., Sreekumar, L., Egeblad, L., Eriksson, S., Chen, L., Veerappan, S., et al. (2018). An efficient proteome-wide strategy for discovery and characterization of cellular nucleotide-protein interactions. PLoS One *13*, e0208273. https://doi.org/10.1371/journal.pone.0208273.

Melhem, H., Spalinger, M.R., Cosin-Roger, J., Atrott, K., Lang, S., Wojtal, K.A., Vavricka, S.R., Rogler, G., and Frey-Wagner, I. (2017). PRDX6 deficiency ameliorates DSS colitis: relevance of compensatory antioxidant mechanisms. J. Crohn's Colitis *11*, 871–884. https://doi.org/10.1093/ecco-jcc/jjx016.

Milani, K.J., Schneider, T.G., and Taraschi, T.F. (2015). Defining the morphology and mechanism of the hemoglobin transport pathway in Plasmodium falciparum-infected erythrocytes. Eukaryot. Cell *14*, 415–426. https://doi.org/10.1128/ec.00267-14.

Mwakingwe, A., Ting, L.-M., Hochman, S., Chen, J., Sinnis, P., and Kim, K. (2009). Noninvasive real-time monitoring of liver-stage development of bioluminescent plasmodium parasites. J. Infect. Dis. *200*, 1470–1478. https://doi.org/10.1086/606115.

Niki, E. (2014). Role of vitamin E as a lipid-soluble peroxyl radical scavenger: in vitro and in vivo evidence. Free Radic. Biol. Med. *66*, 3–12. https://doi.org/10.1016/j.freeradbiomed.2013.03.022.

Noedl, H., Se, Y., Schaecher, K., Smith, B.L., Socheat, D., and Fukuda, M.M. (2008). Evidence of artemisinin-resistant malaria in western Cambodia. N. Engl. J. Med. *359*, 2619–2620. https://doi.org/10.1056/nejmc0805011.

Ohkawa, H., Ohishi, N., and Yagi, K. (1978). Reaction of linoleic acid hydroperoxide with thiobarbituric acid. J. Lipid Res. *19*, 1053–1057. https://doi.org/10.1016/s0022-2275(20)40690-x.

Otsuki, H., Kaneko, O., Thongkukiatkul, A., Tachibana, M., Iriko, H., Takeo, S., Tsuboi, T., and Torii, M. (2009). Single amino acid substitution in Plasmodium yoelii erythrocyte ligand determines its localization and controls parasite virulence. Proc. Natl. Acad. Sci. U S A *106*, 7167–7172. https://doi.org/10.1073/pnas.0811313106.

Pikul, J., and Leszczynski, D.E. (1986). Butylated hydroxytoluene addition improves the thiobarbituric acid assay for malonaldehyde from chicken plasma fat. Food Nahrung *30*, 673–678. https://doi.org/10.1002/food.19860300708.

Preuss, J., Hedrick, M., Sergienko, E., Pinkerton, A., Mangravita-Novo, A., Smith, L., Marx, C., Fischer, E., Jortzik, E., Rahlfs, S., et al. (2012). High-throughput screening for small-molecule inhibitors of plasmodium falciparum glucose-6-phosphate dehydrogenase 6-phosphogluconolactonase. J. Biomol. Screen *17*, 738–751. https://doi.org/10.1177/1087057112442382.

Runas, K.A., and Malmstadt, N. (2015). Low levels of lipid oxidation radically increase the passive permeability of lipid bilayers. Soft Matter *11*, 499–505. https://doi.org/10.1039/c4sm01478b.

Schneider, C.A., Rasband, W.S., and Eliceiri, K.W. (2012). NIH Image to ImageJ: 25 years of image analysis. Nat. Methods *9*, 671–675. https://doi.org/10.1038/nmeth.2089.

Singh, S., Alam, M.M., Pal-Bhowmick, I., Brzostowski, J.A., and Chitnis, C.E. (2010). Distinct external signals Trigger sequential release of apical organelles

during erythrocyte invasion by malaria parasites. PLoS Pathog. *6*, e1000746. https://doi.org/10.1371/journal.ppat.1000746.

Smythe, W.A., Joiner, K.A., and Hoppe, H.C. (2008). Actin is required for endocytic trafficking in the malaria parasite Plasmodium falciparum. Cell Microbiol. *10*, 452–464. https://doi.org/10.1111/j.1462-5822.2007.01058.x.

Spielmann, T., Gras, S., Sabitzki, R., and Meissner, M. (2020). Endocytosis in plasmodium and Toxoplasma parasites. Trends Parasitol. *36*, 520–532. https://doi.org/10.1016/j.pt.2020.03.010.

Tong, L.J., Dong, L.W., and Liu, M.S. (1998). GTP-binding protein mediated phospholipase A2 activation in rat liver during the progression of sepsis. Mol. Cell. Biochem. *189*, 55–61. https://doi.org/10.1023/a:1006804429027.

Tougan, T., Edula, J.R., Morita, M., Takashima, E., Honma, H., Tsuboi, T., and Horii, T. (2020). The malaria parasite Plasmodium falciparum in red blood cells selectively takes up serum proteins that affect host pathogenicity. Malar. J. *19*, 155. https://doi.org/10.1186/s12936-020-03229-1.

Uwimana, A., Umulisa, N., Venkatesan, M., Svigel, S.S., Zhou, Z., Munyaneza, T., Habimana, R.M., Rucogoza, A., Moriarty, L.F., Sandford, R., et al. (2021). Association of Plasmodium falciparum kelch13 R561H genotypes with delayed parasite clearance in Rwanda: an open-label, single-arm, multicentre, therapeutic efficacy study. Lancet Infect. Dis. *21*, 1120–1128. https://doi.org/10.1016/s1473-3099(21)00142-0.

Walliker, D., Quakyi, I.A., Wellems, T.E., McCutchan, T.F., Szarfman, A., London, W.T., Corcoran, L.M., Burkot, T.R., and Carter, R. (1987). Genetic analysis of the human malaria parasite Plasmodium falciparum. Science *236*, 1661–1666. https://doi.org/10.1126/science.3299700.

Wei, L., Adderley, J., Leroy, D., Drewry, D.H., Wilson, D.W., Kaushansky, A., and Doerig, C. (2021). Host-directed therapy, an untapped opportunity for antimalarial intervention. Cell Reports. Med. *2*, 100423. https://doi.org/10.1016/j.xcrm.2021.100423.

WHO. (2021). World Malaria Report 2021 (WHO).

Witkowski, B., Amaratunga, C., Khim, N., Sreng, S., Chim, P., Kim, S., Lim, P., Mao, S., Sopha, C., Sam, B., et al. (2013). Novel phenotypic assays for the detection of artemisinin-resistant Plasmodium falciparum malaria in Cambodia: in-vitro and ex-vivo drug-response studies. Lancet Infect. Dis. *13*, 1043–1049. https://doi.org/10.1016/s1473-3099(13)70252-4.

Wu, Y., Feinstein, S.I., Manevich, Y., Chowdhury, I., Pak, J.H., Kazi, A., Dodia, C., Speicher, D.W., and Fisher, A.B. (2009). Mitogen-activated protein kinase-mediated phosphorylation of peroxiredoxin 6 regulates its phospholipase A2 activity. Biochem. J. *419*, 669–679. https://doi.org/10.1042/bj20082061.

Xie, S.C., Ralph, S.A., and Tilley, L. (2020). K13, the cytostome, and artemisinin resistance. Trends Parasitol. *36*, 533–544. https://doi.org/10.1016/j.pt.2020.03.006.

Zhou, G., Marathe, G.K., Willard, B., and McIntyre, T.M. (2011). Intracellular erythrocyte platelet-activating factor acetylhydrolase I inactivates aspirin in blood. J. Biol. Chem. *286*, 34820–34829. https://doi.org/10.1074/jbc.m111.267161.

STAR★METHODS

KEY RESOURCES TABLE

REAGENT or RESOURCE	SOURCE	IDENTIFIER
Antibodies		
Mouse anti human PRDX6 (1A11)	Santa Cruz Biotechnology	Cat# sc-59671; RRID: AB_632188
Goat anti human Hemoglobin HRP-coupled	Bethyl	Cat# A80-134P; RRID: AB_67041
Rat anti mouse CD71 APC	Thermo Fisher Scientific	Cat# 17-0711-80; RRID: AB_1834356
Rabbit anti-*Pf*NAPL	Singh et al., 2010	N/A
Goat anti mouse HRP-coupled	Promega	Cat# W4021; RRID: AB_430834
Goat anti rabbit HRP-coupled	Promega	Cat# W4011; RRID: AB_430833
Goat anti mouse Alexa Fluor 488-coupled	Thermo Fisher Scientific	Cat# A-11029; RRID: AB_2534088
Protein A gold 10nm	UMC Utrecht	Cat# PAG 10 nm 200μL
Rabbit Anti-Mouse Immunoglobulins	Dako/Agilent	Cat# Z0259; RRID: AB_2532147
Bacterial and virus strains		
E. Coli BL21 (DE3)	Sigma	Cat# CMC0014
Chemicals, peptides, and recombinant proteins		
Darapladib	SelleckChem	Cat# S7520
ATK	Cayman	Cat# 62120
MAFP	Enzo	Cat# BML-ST360
Varespladib (LY3115920)	Cayman	Cat# 18267
P11	Cayman	Cat# 17507
Alpha-Tocopherol	Sigma	Cat# T3251
Dihydroartemisinin	Cayman	Cat# 19846
E64	Sigma	Cat# E3132
BODIPY 581/591 C11	Invitrogen	Cat# D3861
LysoSensor™ Yellow/Blue dextran, 10,000 MW	Invitrogen	Cat# L22460
SYTO 61	Invitrogen	Cat# S11343
SYBR Green I	Lonza	Cat# 50513
Hoechst 33342	Invitrogen	Cat# H3570
TAMRA-FP ABPP Probe	Invitrogen	Cat# 88318
SYPRO Orange	Invitrogen	Cat# S6651
[^{14}C]-DPPC	American Radiolabeled Chemicals	Cat# ARC0715-10UCI
Cholesterol	Sigma	Cat# C8667
DPPC	Avanti Lipids	Cat# 850355P
Egg-yolk PC	Sigma	Cat# P8318
Egg-yolk PG	Sigma	Cat# P3556
UltimaGold liquid scintillation cocktail	Perkin Elmer	Cat# 6013179
Saponin	Sigma	Cat# 47036
Mg-ATP	Sigma	Cat# A9187
Recombinant MAPK (ERK2)	R&D Systems	Cat# 1230-KS
Recombinant PRDX6	This study	N/A
Recombinant *Pf*GluPho	Laboratory of Katja Becker, Gießen, Germany (Jortzik et al., 2011)	N/A
$NADP^+$	Cayman	Cat# 10004675
Glucose-6-phosphate	Sigma	Cat# G7879
Butylated hydroxytoluene (BHT)	Sigma	Cat# B1378
2-thiobarbituric acid (TBA)	Sigma	Cat# T5500

(*Continued on next page*)

Continued

REAGENT or RESOURCE	SOURCE	IDENTIFIER
OsO_4	Electron Microscopy Sciences	Cat# 19150
EMbed-812 epoxy resin	Electron Microscopy Sciences	Cat# EMS #14120
Deposited data		
Raw mass spectrometry proteomics data from CETSA	This study: ProteomeXchange Consortium via the JPOSTrepo partner repository	Accession number: PXD029803
Raw western blots and fluorescent gel images	This study; Mendeley Data	https://doi.org/10.17632/57j6y7vfhk.1
Raw flow cytometry data	This study; Mendeley Data	https://doi.org/10.17632/57j6y7vfhk.1
Experimental models: Cell lines		
0+ Red blood cells (in citrate buffer)	ICAReB, Institut Pasteur	N/A
Plasmodium falciparum 3D7	Walliker et al., 1987	N/A
Plasmodium falciparum NF54 K13 C580Y	Ariey et al., 2014	N/A
Plasmodium falciparum field isolate 3815	Ariey et al., 2014	N/A
Plasmodium falciparum field isolate 3601	Ariey et al., 2014	N/A
Plasmodium yoelii YM lethal strain	Mwakingwe et al., 2009	N/A
Experimental models: Organisms/strains		
Mouse: C57/BL6JRj WT	Janvier Labs	Cat# SA-CJ-11M
Mouse: B6.129-*Prdx6*^{tm1Abf}/Mmjax	Laboratory of Aron B. Fisher, UPenn, USA	Cat# 043402-JAX
Recombinant DNA		
Plasmid: 6x-His tagged human PRDX6 in pET28a vector	GenScript, USA	N/A
Software and algorithms		
GraphPad Prism 9.2.0	Graph Pad Software	N/A
ImageJ 1.53c	Open Source, (Schneider et al., 2012)	https://imagej.nih.gov/ij/
GIMP 2.10.12	OpenSource	https://www.gimp.org
Inkscape 0.92	OpenSource	https://inkscape.org/
mineCETSA	Open Source	https://github.com/nkdailingyun/mineCETSA
R	Open Source, R Core Team	https://www.R-project.org
R Studio	Open Source, RStudio Team	http://www.rstudio.com/
FlowJo 10.8	FlowJo, LLC	N/A
Other		
Percoll	GE Healthcare	Cat# 17-0891-01

RESOURCE AVAILABILITY

Lead contact

Further information and requests for reagents should be directed to and will be fulfilled by the lead contact, Chetan Chitnis (chetan.chitnis@pasteur.fr).

Materials availability

This study did not generate new unique reagents.

Data and code availability

- The mass spectrometry proteomics data have been deposited to the ProteomeXchange Consortium via the JPOSTrepo partner repository with the dataset identifier PXD029803.
- Original western blot and fluorescent gel images, as well as raw flow cytometry data have been deposited at Mendeley and are publicly available as of the date of publication. The DOI is listed in the key resources table.
- Microscopy data reported in this paper will be shared by the lead contact upon request.
- This study did not generate new code.
- Any additional information required to reanalyze the data reported in this paper is available from the lead contact upon request.

EXPERIMENTAL MODEL AND SUBJECT DETAILS

Plasmodium falciparum parasites

All *Plasmodium falciparum* strains were cultured at a final hematocrit of 2–4% under mixed gas atmosphere (5% O_2, 5% CO_2 and 90% N_2) at 37°C. *P. falciparum* 3D7 (Walliker et al., 1987) was cultured in RPMI-1640 medium with 0.5% Albumax (complete RPMI, cRPMI) using O^+ human erythrocytes (ICAReB, Institut Pasteur Paris, France). ART-resistant parasite strains *P. falciparum* $NF54^{C580Y}$ (Ariey et al., 2014) and the field isolates Cambodia 3815 and 3601 (Ariey et al., 2014) were cultured in RPMI supplemented with 0.5% Albumax and 2.5% AB^+ human serum (EFS, Rungis, France) using O^+ human erythrocytes.

Red blood cells

O^+ human erythrocytes in citrate buffer were obtained commercially from ICAReB, Paris, France.

In vivo infection of mice with *P. yoelii*

prdx6$^{-/-}$ mice were generated from C57/BL6JRj mice in the lab of Aron B. Fisher, University of Pennsylvania, USA as described earlier and are available under the accession number B6.129-*Prdx6*^{tm1Abf}/Mmjax (Feinstein, 2019). Animals were housed in the Institut Pasteur animal facilities accredited by the French Ministry of Agriculture for performing experiments on live rodents. Work on animals was performed in compliance with French and European regulations on care and protection of laboratory animals (EC Directive 2010/63, French Law 2013–118, February 6th, 2013). All experiments were approved by the Ethics Committee #89 and registered under the reference 01324.02 and dap180040. At the time of the experiment, both *prdx6*$^{-/-}$ mice and WT mice were about 44 weeks of age and littermates of both sexes were randomly assigned to experimental groups.

prdx6$^{-/-}$ mice and age-matched control C57/BL6JRj WT mice (Janvier Labs, France) were infected with the *P. yoelii* YM lethal strain (Mwakingwe et al., 2009) via the tail vein for an initial parasitemia of 0.002%. Parasitemia was measured by Giemsa-stained blood smears and by flow cytometry. For this, *P. yoelii* YM cells were labelled with 5× SYBR Green I and 1:100 α-mouse CD71-APC (eBioscience, UK) for 30min at 37°C. To specifically assess intraerythrocytic growth, $CD71^+$ reticulocytes were excluded. Infected mature RBCs were identified as SYBR $Green^+$ and $CD71^-$ cells.

METHOD DETAILS

Lysis with saponin and sample preparation

Late trophozoites and early schizonts from synchronous *P. falciparum* 3D7 cultures were purified with a Percoll gradient. The resulting parasite pellet was resuspended in PBS. RBC membranes were lysed by exposure to 0.01% Saponin (Sigma, Stock 1% in H_2O) for 5 min at RT. Complete hemolysis was confirmed by Giemsa-stained blood smears. After washing two times with PBS, the hemolysed pellet was either assessed by mass spectrometry (cf. respective method) or immunoblotting. For immunoblotting, the pellet was resuspended in 1× Laemmli SDS sample buffer (BioRad) with 200mM DTT (Sigma) and boiled at 95°C for 10 min.

SDS-PAGE and immunoblotting

Samples were separated on SDS-polyacrylamide gel and proteins were transferred onto a nitrocellulose membrane (GE healthcare) using a wet transfer system (BioRad). The membrane was blocked in PBS with 5% skimmed milk overnight at 4°C with continuous agitation. Following this, the membranes were incubated with mouse monoclonal antibody against human PRDX6 (α-hPRDX6 1A11 (1:2000), Santa Cruz), rabbit antisera raised against *P. falciparum* nucleosome assembly protein L (α–*Pf*NAPL 1:500) (Singh et al., 2010) and goat antisera against human hemoglobin (α-hHb HRP 1:5000, Bethyl) in PBS with 2.5% skimmed milk and 0.05% Tween 20 for 2h at RT. After washing, blots with α-PRDX6 and α-*Pf*NAPL were incubated with respective α-mouse and α-rabbit horseradish peroxidase (HRP)-coupled secondary antibodies (1:5000, Promega) for 1h at RT. Membranes were developed with enhanced chemiluminescence (ECL) substrate (ThermoFisher Scientific) and imaged on an Amersham Imager 600 (GE Healthcare). Band intensity was calculated using ImageJ software (NIH, Bethesda, USA) (Schneider et al., 2012).

Immunofluorescence microscopy

P. falciparum 3D7 was cultured as described above and mice were infected with *P. yoelii* YM as described below. 1mL of a 4% hematocrit, high parasitemia culture for *P. falciparum* or 20μL of freshly drawn blood in EDTA for *P. yoelii* YM was pelleted by centrifugation (1.5 g, 3min, RT) and resuspended in freshly prepared PBS containing 4% paraformaldehyde (Electron Microscopy Sciences) and 0.0075% gluteraldehyde (Sigma) and fixed for 30 min at RT. After washing in PBS once, fixed parasites were permeabilized with 0.1% Triton X-100 in PBS for 10 min at RT. Cells were washed in PBS again and blocked for 30 min in PBS with 2.5% BSA. Antibody dilutions were prepared in PBS with 2.5% BSA. After blocking, parasites were incubated with mouse α-hPRDX6 1A11 (1:500, Santa Cruz) for 1h at RT. Parasites were washed twice in PBS and incubated with α-mouse AlexaFluor 488-coupled secondary antibody (1:2000, Invitrogen) and Hoechst 33342 (2 μM final) (Invitrogen), washed again twice in PBS and resuspended in 30 μL PBS. From this suspension, 4 μL was transferred onto a glass slide and covered with a glass coverslip. Samples were examined under a widefield Deltavision Elite high resolution fluorescence microscope (GE Healthcare Lifesciences) using DAPI, FITC and differential interference contrast (DIC) channels. The images were deconvolved using the Deltavision software default

setting (10 iterations). The integrated fluorescence density (IDF) and area of both the parasite as well as the whole infected RBC were measured in multiple z-planes using ImageJ software (NIH, Bethesda, USA). To quantify the localization of PRDX6 within the parasite, the integrated fluorescence density (IFD) and area of both the parasite as well as the whole infected RBC were measured in multiple z-planes. For each z-plane, the relative IFD of the parasite within the infected RBC was divided by the relative area of the parasite within the infected RBC to calculate the relative mean fluorescent signal located within the parasite as compared to the whole RBC: $(IFD_{Parasite}/IFD_{iRBC})/(Area_{Parasite}/Area_{iRBC})$. Finally, the average of all measured z-planes for a single parasite was calculated. Hemozoin crystal size was measured in DIC images using ImageJ.

Transmission electron microscopy

Fixation

1 mL of *P. falciparum* 3D7 culture was pelleted by centrifugation (1500g, 3 min, RT) and resuspended in freshly prepared PBS containing 4% EM-grade para-formaldehyde (PFA, Electron Microscopy Sciences) and 0.1% EM-grade GA (Sigma) and fixed for 1 h on ice. After washing in PBS once, fixed parasites were stored in PBS with 1% PFA at 4°C.

Immuno-TEM

Fixed parasites were washed three times in PBS followed by incubation for 15min in 50mM NH_4Cl at RT. Parasites were resuspended in PBS with 10% gelatin (Sigma) and incubated for 10 min at 37°C. The samples were allowed to solidify on ice and were infiltrated with 2.3M sucrose at 4°C overnight, mounted onto sample pins and frozen in liquid nitrogen. Subsequently, the samples were cryosectioned (60 nM thickness) using a FC6/UC6 cryo-ultramicrotome (Leica) and a 35° diamond knife (Diatome). The sections were picked up using a 1:1 mixture of 2% methyl cellulose (Sigma) and 2.3M sucrose. Samples were quenched with 50 mM NH_4Cl, blocked in PBS with 1% BSA and immunolabeled with α-hPRXD6 1A11 (SantaCruz, 1:20) IgG1a monoclonal antibody in PBS with 1% BSA followed by a bridge step labelling with a polyclonal Rabbit Anti-Mouse Immunoglobulins (Dako, 1:50) and protein A-gold 10 nm (UMC Utrecht, 1:50) treatment for 15 min. Finally, samples were fixed with 1% glutaraldehyde in PBS for 5 min. The sections were thawed and stained/embedded in 4% uranylacetate/2% methyl cellulose mixture (1:9). Images were recorded with a Tecnai Spirit transmission electron microscope at 120 kV with bottom-mounted EAGLE 4Kx4K camera.

EPON resin embedding

Fixed parasites were treated again with 2.5% gluteraldehyde (Sigma) in PBS overnight, washed three times in PBS and mordanted with tannic acid 1% in PBS for 30min at RT. Cells were then washed three times in PBS, postfixed with 1% OsO_4 for 1.5 h and washed three times with distilled water and stored overnight at 4°C. Samples were dehydrated 15 min in a graded series of ethanol (25%, 50%, 75%, 95%, 3 × 100%). Samples were incubated 1 × 15min, then 2 × 10min in propylene oxide and embedded in EMbed-812 epoxy resin (EMS; EPON/Propylene Oxide: r = 25/75 for 2 h; r = 50/50 overnight; r = 75/25 all the day and overnight with the tubes open under the chemical hood). Samples were then embedded 3 × 2h at RT in pure EPON and subjected to heat polymerization for 5 days at 60°C. Thin sections were cut with a Leica Ultramicrotome Ultracut UC7′ sections (60 nm), stained with uranyl acetate and lead citrate. Images were recorded with a Tecnai Spirit transmission electron microscope at 120 kV with bottom-mounted EAGLE 4Kx4K camera (FEI-Thermofisher).

Recombinant expression of human PRDX6

A synthetic gene encoding human PRDX6 was tagged with a 6x-His tag, codon-optimized for expression in *E. coli* was synthesized and cloned into the *E. coli* expression vector pET28a (GenScript, Piscataway, USA). The plasmid vector was transformed into *E. coli* BL21 (DE3) competent cells (Sigma). A single colony of transformed bacteria was picked from a LB-agar plate with Kanamycin (50 μg/mL) and grown in LB medium with Kanamycin at 37°C to an optical density of OD_{600} of 0.6. Expression of recombinant PRDX6 was induced with 1mM isopropyl β-d-thiogalactopyranoside (IPTG, Sigma). The culture was incubated for 20h at 18°C, bacteria were harvested by centrifugation (6000 g, 10 min, 4°C) and resuspended in lysis buffer (50 mM Tris/HCl at pH 8, 150 mM NaCl, 2 mM β-mercaptoethanol). After sonication and removal of cell debris by centrifugation, the supernatant was loaded onto a HisTrap FF affinity column (GE Healthcare) and equilibrated with lysis buffer (see above). Recombinant PRDX6 was eluted with lysis buffer supplemented with 250 mM imidazole (Sigma). Subsequently, recombinant PRDX6 was purified by gel filtration chromatography on a Superdex 200 16/600 column (Sigma) equilibrated with 20mM HEPES at pH 7.0, 2mM EDTA and 1mM DTT. The yield from a 1L initial bacterial culture was about 12.5 mg of purified recombinant PRDX6.

Activity-based protein profiling of PRDX6

Recombinant human PRDX6 was diluted to 10 mg/mL in PBS. Aliquots of 50 μL were incubated for 5 min at RT with different concentrations of Darapladib (SelleckChem, USA), Varespladib (Cayman Chemical, USA), MAFP (Cayman Chemical, USA), ATK (Cayman Chemical, USA), P11 (Cayman Chemical, USA) or DMSO. TAMRA-fluorophosphonate (TAMRA-FP, Invitrogen, Thermo Fisher, USA) was solved in DMSO (100 μM), added to the sample (2 μM final) and incubated for 30min at 37°C. After 30min, the reaction was quenched by addition of 15 μL 4×Laemmli sample buffer and 7.5 μL 1M DTT. The sample was heated to 95°C for 10 min and separated by SDS-PAGE on a 12% SDS polyacrylamide gel. After electrophoresis, the gel was imaged on a ChemiDoc MP imager (BioRad, USA) in the Cy3 channel.

PRDX6 phosphorylation and PLA_2 activity assay

PRDX6 was phosphorylated according to the method described by Wu et al. (Wu et al., 2009). Recombinant human PRDX6 (150 μg/mL final) and active MAPK (ERK2, R&D Systems, 10 μg/mL final) were added to 30 μL of a phosphorylation buffer containing 50 mM Tris/HCl pH 7.5, 20 μM EGTA, 10 mM $MgCl_2$ and 2 mM Mg-ATP (Sigma) and were incubated for 90 min at 30°C.

Measurement of PLA_2 activity of phosphorylated PRDX6 (pPRDX6) was based on the enzymatic PLA_2 assay described by Wu et al. (Wu et al., 2009) and the rapid free fatty acid extraction method by Katsumata et al. (Katsumata et al., 1986). Liposomes consisting of DPPC/egg yolk PC/egg yolk PG/cholesterol (6:3:1.2:0.95, DPPC from Avanti Polar Lipids, all other Sigma) with 0.6 μCi tracer [2-palmitoyl-1-^{14}C]-dipalmitoyl phosphatidylcholine (^{14}C-DPPC, American Radiolabeled Chemicals) were prepared by freezing/thawing three times in liquid nitrogen. 100 μL diluted phosphorylated PRDX6 (2.5 μg/mL in PLA_2 assay buffer 40 mM NaOAc, 5 mM EDTA, pH 5), or blank PLA_2 assay buffer was added to 800 μL PLA_2 assay buffer containing different concentrations of Darapladib in DMSO. After addition of 100 μL liposome preparation, the samples were incubated for 2 h at 37°C. The enzymatic reaction was terminated by addition of 200 μL 5% Triton X-100 in PLA_2 assay buffer. The product of the PLA_2 enzymatic reaction, free ^{14}C-palmitic acid, was extracted by addition of 10 mL hexane with 0.1% acetic acid (v/v) and 200 mg of anhydrous Na_2SO_4 (Tong et al., 1998) and subsequent vortexing for 20s. 3 mL of the hexane layer was added to 10 mL UltimaGold liquid scintillation cocktail (PerkinElmer, Waltham, USA) and measured on a TriCarb 2800TR liquid scintillation counter (PerkinElmer, Waltham, USA).

Parasite progression and growth assay

General assay description

To assess the effect of inhibitors on the ring to schizont progression, and growth from ring stage to next generation ring stage, a tightly Percoll-synchronised culture with about 2% parasitemia and 2% hematocrit was treated with different inhibitors at ring stage (14–20 hpi). The inhibitors were present throughout the assay. The concentration of the solvent was kept equal in all samples in a given experiment and maintained below 0.1% to avoid toxic effects. For each condition, a triplicate set of 1 mL cultures was added into wells of a 24-well plate and kept at 37°C and 5% O_2, 5% CO_2 throughout the assay. The initial ring stage culture was scored by flow cytometry as described below and by examination of Giemsa-stained blood smears. After 20h, the samples were measured again to assess progression to schizont stage. Further 24h later, the overall growth and development of next generation rings was measured. Flow cytometry data was analyzed with the FlowJo 10.8 software (FlowJo LLC). After exclusion of doublets, a gate for uninfected and infected RBCs based on the size of the cells in the FSC-A channel was set up to exclude debris and merozoites. Finally, gates for rings, trophozoites and multiply infected RBCs, and schizonts were set up. The total parasitemia was defined as the sum of the aforementioned gates. Each experiment was performed with three biological replicates. Relative rate of progression was calculated as the fraction of schizonts in treated and control samples (T/C). Relative growth was calculated as the ratio of parasitemia in the treated and control samples after subtraction of the initial parasitemia (T-I/C-I).

Labelling of P. falciparum for flow cytometry

Cultures were diluted to 0.2% hematocrit and transferred to a 96-well round bottom plate. 5 μL of 200× SYBR Green I (Lonza, Switzerland) was added to 200 μL of the diluted culture for a final concentration of 5× SYBR Green I. The plate was then incubated for 30 min at 37°C in the dark. Samples were measured on a calibrated MACSquant flow cytometer on the forward scatter (FSC), side scatter (SSC) and B1 fluorescent channel (B1: λ_{Ex} 488 nm and λ_{Em} 525/50 nm). Data was processed with the FlowJo 10.8 Software (FlowJo, LLC).

Infection of mice with *P. yoelii*

prdx6$^{-/-}$ mice and age-matched control C57/BL6JRj WT mice (Janvier Labs, France) were infected with the *P. yoelii* YM lethal strain (Mwakingwe et al., 2009) via the tail vein for an initial parasitemia of 0.002%. Parasitemia was measured by Giemsa-stained blood smears and by flow cytometry. *P. yoelii* YM cells were labelled with 5× SYBR Green I and 1:100 α-mouse CD71-APC (eBioscience, UK) for 30min at 37°C. To specifically assess intraerythrocytic growth, CD71$^+$ reticulocytes were excluded. Infected mature RBCs were identified as SYBR Green$^+$ and CD71$^-$ cells.

Ex vivo P. yoelii YM progression assay

prdx6$^{-/-}$ mice and age-matched control C57/BL6JRj WT mice were infected with *P. yoelii* YM as described above. When the parasitemia in the mice reached about 20%, 20μL blood was drawn from the chin and collected in heparinized tubes. 15μL of the blood was diluted in 8 mL of RPMI-1640 medium with 0.5% Albumax (cRPMI) and added in 1mL aliquots into a 24-well plate. The initial amount of schizonts was measured by Giemsa-stained blood smears and flow cytometry by labelling the parasites with 5× SYBR Green I and 1:100 α-mouse CD71-APC for 30min at 37°C. Infected mature erythrocytes were identified as SYBR Green$^+$ and CD71$^-$ cells. CD71$^+$ reticulocytes were excluded by gating. Cells were treated with Darapladib (0.5 and 1μM) or DMSO and incubated for 16 h at 37°C, 5% O_2 and 5% CO_2 to allow progression of parasites to schizont stage. After 16 h, schizont development in RBCs was assessed by Giemsa-stained blood smears and flow cytometry as described above.

Mass spectrometry detection

Mature trophozoite stage (26–38hpi) 3D7 *P. falciparum* parasites were liberated from host cells with 0.01% ice-cold Saponin (w/v) and washed thoroughly with ice-cold PBS. The parasite pellet was resuspended in lysis buffer (50mM HEPES pH7.5,

5mM beta-glycerophosphate, 0.1mM Na_3VO_4, 10mM $MgCl_2$, 2mM TCEP and cocktail EDTA-free protease inhibitors (Sigma) and homogenized at 4°C in Precellys Cryolys Evo Tissue homogoenizer (Bertin Instruments). The soluble protein fraction was isolated by centrifugation, reduced and denaturated in 100mM TEAB, 20mM TCEP, 0.05% (w/v) RapiGest at 55°C for 20min, alkylated with 55mM CAA at RT for 30 min, digested with LysC (0.05μg of LysC/μg of protein) for 4h and followed by trypsin digestion for 18h at 37°C. Peptides were labelled with TMT10plex Isobaric Label Reagent Set (Pierce), desalted using Oasis HLB cartidges (Waters) and subjected to a reversed-phase fractionation on a 0%–90% Acetonitrile in 10mM Ammonium Formate (pH10) gradient. Twenty 1μg fractions were subsequently analyzed by Q-Exactive HF LC-MS/MS system (Thermo Scientific) for each replicate sample. Raw data was analysed using SEQUEST in Proteome Discoverer 2.1 (Thermo Scientific) against combined human (Uniprot) and *P. falciparum* (PlasmoDB) reference proteome databases with 25 ppm precurson mass tolerance, 0.05 Da fragment mass tolerance with Decoy database search using 0.01 and 0.05 strict and relaxed target FDR cutoffs respectively. The searches included static modifications: TMT6plex on N-terminus and K, Carbamidomethylation on C, and dynamic modifications Acetylation on N-terminus, Oxidation on M, and Deamination on N and Q.

MS-IDTR-CETSA and analysis

The assay was carried out in two biological replicates, as described with minor modifications (Dziekan et al., 2020). In brief, lysate from saponin-liberated mature (32 ± 6 hpi) *P. falciparum* parasites was incubated for 3min with different concentrations (1.5nM–100μM) of Darapladib (MedChemExpress) or the DMSO control and subsequently heated for 3min to 50°C, 55°C or 60°C to denature unstable protein subsets, or incubated at 37°C. Soluble protein fractions were isolated by centrifugation and analysed by quantitative mass spectrometry as described before (Dziekan et al., 2020). Data analysis was carried out in R environment using mineCETSA package. Resulting protein stability profiles under thermal challenge conditions (i.e. > 37°C) were evaluated based on observed change in protein stability [reading delta Area Under the Curve (ΔAUC) relative to the non-denaturing (37°C) condition, the Fold Change (FC) in protein abundance relative to vehicle control treated sample], as well as protein stability profile adherence to expected sigmoidal shape of dose response (R^2). The criteria used for identification of drug-dose dependent changes in protein stability are characterized by ΔAUC surpassing two and a half times Median Absolute Deviation (MAD) for the dataset and $R^2 > 0.8$. ITDR CETSA mass spectrometry proteomics data have been deposited to the ProteomeXchange Consortium via the JPOSTrepo partner repository with the dataset identifier PXD029803.

Differential scanning fluorimetry of PRDX6

Melt curves of recombinant PRDX6 with and without inhibitors were determined using differential scanning fluorimetry. The assay was conducted 384-well plates with a final volume of 10μL. A PBS-based solution of PRDX6 (2μM) and SYPRO Orange (5x) was incubated for 60min at RT with 25μM Darapladib, 25μM Varespladib or DMSO. Melt curves were determined on a BioRad CFX384 qPCR thermocycler (40–70°C at 1.2°C/min, FRET Channel). Data was analysed using the CFX manager software (BioRad).

Recombinant expression of *P. falciparum* GluPho

Recombinant N-terminal His_6-tagged *P. falciparum* glucose-6-phosphate dehydrogenase-6-phosphogluconolactonase (*Pf*GluPho) was produced according to Jortzik et al. (Jortzik et al., 2011) in the vector pQE30 in *E. coli* M15 cells (Qiagen) with pRAREII (Novagen).

Glucose-6-phosphate dehydrogenase activity assay

Glucose-6-phosphate dehydrogenase (G6PD) activity of recombinant *Pf*GluPho was measured by monitoring the reduction of $NADP^+$ to NADPH at ex340/em460 nm in a 96-well formate as described before (Preuss et al., 2012). Recombinant *Pf*GluPho (0.4 μg/mL) was added to a reaction mixture containing 0.05 M Tris (pH 7.5), 3.3 mM $MgCl_2$, 0.005% Tween 20, 1 mg/mL BSA and the substrates $NADP^+$ (20 μM, Cayman) and glucose 6-phosphate (G6P, 25 μM, Sigma) close to the K_M. Linear reaction curves were monitored over 10 min, and IC_{50} values calculated with GraphPad Prism. Samples without glucose-6-phosphate (G6P) were used to control the specificity of the reaction.

Parasite lysate was prepared by sonication of Saponin (0.01%) liberated trophozoite stage *P. falciparum* 3D7 parasites. Briefly, *P. falciparum* lysate was added to a reaction mixture containing 0.1 M Tris/HCl (pH 8.0), 10mM $MgCl_2$, 0.5mM EDTA and 200μM $NADP^+$. 200μM of G6P were added as a substrate and the enzyme activity was measured on a Tecan infinite M1000 Pro plate reader at 340nm. To correct for background activity in the parasite lysate and to assess specificity of the reaction, samples without G6P substrate were measured.

Lipid peroxidation measurement with BODIPY$^{581/591}$ C11

To measure oxidative stress, parasites were labelled with the fluorescent lipid peroxidation sensor BODIPY$^{581/591}$ C11 (Invitrogen, Thermo Fisher, USA) based on the method described by Fu et al. (Fu et al., 2009). A *P. falciparum* 3D7 culture was highly synchronized via repeated Percoll gradient purifications. Parasites were treated with 0.5 μM or 2 μM Darapladib, 10 μM Varespladib or DMSO for 2h at late trophozoite/early schizont stage (38–42 hpi). After treatment for 2 h, parasites were pelleted by centrifugation and resuspended in labelling solution (5 μM BODIPY$^{581/591}$ C11, 10 μM Hoechst 33342 in cRPMI) and incubated for 1 h at 37°C, 5% O_2, 5% CO_2. Parasites were measured on a MACSquant flow cytometer: BODIPY$^{581/591}$ C11 reduced, λ_{Ex} 488nm, λ_{Em} 614/50nm, "Red"; BODIPY$^{581/591}$ C11 oxidised λ_{Ex} 488nm, λ_{Em} 525/50 nm, "Green"; Hoechst 33342, λ_{Ex} 405nm, λ_{Em} 450/50 nm. Data was analyzed

using FlowJo 10 (FlowJo, LLC). After exclusion of doublets, debris and merozoites by size, infected RBCs were gated for by selecting Hoechst 33342 positive cells. The MFI of "Red" and "Green" channels of infected RBCs was calculated. Lipid peroxidation was calculated as $MFI_{Green}/(MFI_{Green} + MFI_{Red})$. Relative lipid peroxidation was calculated as the ratio of lipid peroxidation in treated and control parasites (T/C).

TBARS assay

Detection of thiobarbituric acid reactive substances (TBARS), such as malondialdehyde (MDA), was adapted from the method published by Ohkawa et al. (Ohkawa et al., 1978). To quench auto-oxidation, butylated hydroxytoluene (BHT, Sigma) was added to the reaction (Pikul and Leszczynski, 1986). A 0.8% (w/v) aqueous solution of 2-thiobarbituric acid (TBA, Sigma) was prepared by heating the solution to 50°C for 2h. A 20% parasitemia, 4% hematocrit *P. falciparum* 3D7 culture, or a 4% hematocrit RBC suspension were treated with 0.5μM or 2μM Darapladib, or DMSO for 8h at 37°C, 5% O_2, 5% CO_2. Afterwards, 5mL of each culture was pelleted by centrifugation. The pellet was resuspended in a 15 mL reaction tube with 1.5 mL 20% acetic acid pH 3.5 (v/v, Sigma), 200μL 10% SDS (Sigma), 100μL of 0.1% (w/v) BHT in EtOH, 1.5mL of 0.8% TBA in H_2O and 600 μL H_2O for a total reaction volume of 4 mL. The samples were heated for 1 h in vigorously boiling water. To stop the reaction, the reaction mix was cooled down in an ice bath. The pink colored reaction product was extracted by addition of 5 mL 1-butanol (Sigma), vortexing and centrifugation (2000 g, 10min, RT). 150μL of the butane layer was transferred into a black-walled 96-well plate and fluorescence (λ_{Ex} 530 nm, λ_{Em} 550 nm) was measured on a Tecan Infinite M1000 Pro plate reader.

Host cell cytosol uptake assays

Host cell cytosol uptake assay with E64

A synchronous *P. falciparum* 3D7 culture at ring stage was treated with 2 μM Darapladib, 20 μM E64, a combination of both, or DMSO as control and incubated overnight at 37°C, 5% O_2, 5% CO_2 until control parasites progressed to schizonts. Cells were observed by light microscopy of Giemsa-stained blood smears and transmission electron microscopy of EPON resin embedded parasites as described above.

Host cell cytosol uptake assay with LysoSensor Y/B

RBCs were preloaded with the pH-sensitive LysoSensor Yellow/Blue Dextran 10kD (Invitrogen) based on the method described by Jonscher et al. (Jonscher et al., 2019). Briefly, fresh RBCs (stored less than a week) were washed three times in cold PBS. Of this pellet, 64 μL packed RBCs were transferred to 128 μL of freshly prepared preloading lysis buffer (5 mM K_2HPO_4, 20 mM Glucose, pH 7.4) and 2 μL 30mM DTT, 4 μL 50mM Mg-ATP (Sigma) and 2 μL of 50mg/mL LysoSensor Blue/Yellow dextran 10kD (Invitrogen) on ice. The suspension was rotated at 4°C for 10min. For resealing, 50 μL of 5× resealing buffer (750 mM NaCl, 25 mM Na_2HPO_4, pH 7.4) was carefully added to the RBC suspension and incubated for 60 min at 37°C while gently rocking. Preloaded RBCs were washed three times in cRPMI and resuspended in 1 mL cRPMI.

For infection of preloaded RBCs, schizonts were isolated from 30 mL of a 4% hematocrit highly synchronous, late stage *P. falciparum* 3D7 culture using a Percoll gradient. The resulting schizont pellet was resuspended in 1 mL cRPMI, mixed with the 1 mL preloaded RBCs and cultured for 20h at 37°C, 5% O_2, 5% CO_2 to allow re-invasion and formation of rings. Successful re-invasion was controlled with Giemsa-stained blood smears and flow cytometric measurement as described above. At ring stage, the culture was split into two parts and treated with either 2 μM Darapladib or DMSO control and further incubated until control parasites progressed to late trophozoite stage (32–40hpi, large hemozoin crystals visible). To identify infected RBCs, the cells were stained with 0.5 μM SYTO 61 (Invitrogen) for 30min at 37°C and washed once in cRPMI. The resulting pellet was resuspended in cRPMI and transferred onto a glass slide and covered with a glass coverslip. Images were taking with Deltavision Elite high resolution fluorescence microscope (GE Healthcare Lifesciences): LysoSensor pH 7, λ_{Ex} 390/18 nm, λ_{Em} 435/48, "Blue"; LysoSensor pH 5, λ_{Ex} 390/18 nm, λ_{Em} 597/45, "Yellow"; SYTO 61, λ_{Ex} 632/22 nm, λ_{Em} 679/34 and differential interference contrast (DIC). Fluorescent signal in the FV was quantified as the integrated density of the FV area in the "Yellow" and "Blue" channels using ImageJ. Relative successful transport of cytosolic LysoSensor to the FV was expressed as the ratio of integrated densities of "Yellow" and "Blue" channels.

For flow cytometric measurement, the cells were stained with 0.5 μM SYTO 61 for 30 min at 37°C, washed once in cRPMI afterwards and measured on a MACSquant flow cytometer: LysoSensor pH 7, λ_{Ex} 405 nm, λ_{Em} 450/50 nm, "Blue"; LysoSensor pH 5, λ_{Ex} 405 nm, λ_{Em} 525/50 nm, "Yellow" and SYTO 61, λ_{Ex} 561 nm, λ_{Em} 695/50 nm. Data was analyzed using FlowJo 10 (FlowJo, LLC). Briefly, after exclusion of doublets, debris and merozoites by size, infected RBCs were gated for by selecting SYTO 61 positive cells. The MFI of "Yellow" and "Blue" channels of SYTO 61^+ infected RBCs was calculated. Relative successful transport of cytosolic LysoSensor to the FV was expressed as the ratio of the MFI of "Yellow" and "Blue" channels.

Artemisinin ring stage survival assay

Ring stage survival upon treatment with Dihydroartemisinin (DHA, Cayman Chemical) was measured based on the method described by Witkowski et al. (Witkowski et al., 2013). Briefly, ring stage survival was assessed in *P. falciparum* NF54 K13 C580Y and ART-resistant *P. falciparum* field isolate strains 3815 and 3801. Late stage schizonts were purified from synchronous *P. falciparum* cultures which contained only late stage (44–48 hpi) schizonts and newly invaded rings. Purified schizonts were added to fresh RBCs and the culture was incubated for 3 h at 37°C, to allow egress, re-invasion and development of rings. After 3h, unegressed schizonts

were removed by a second Percoll purification. The pellet containing highly synchronous 0–3 h old rings and RBCs was washed in cRPMI and was examined by flow cytometry and Giemsa-stained blood smears to confirm schizont depletion and to measure the parasitemia. Subsequently, the parasitemia was adjusted to 1% and the culture diluted 1:10 in cRPMI. Initial parasitemia was measured by flow cytometry as described above and Giemsa-stained blood smears. In a 24-well plate, 1 mL aliquots of the cultures were treated with 700 nM DHA, 1μM Darapladib, or combinations of both drugs for 6h at 37°C, 5% O_2, 5% CO_2. The concentration of DMSO was kept equal in all samples. After 6 h, the drugs were removed by washing twice in cRPMI. After resuspension in cRPMI, the cultures were incubated for further 66 h and parasitemia was assessed by flow cytometry using SYBR Green I as described before and Giemsa-stained blood smears. Parasite survival was calculated as the ratio of rings in the treated and control samples after subtraction of the initial amount of rings (T-I/C-I).

QUANTIFICATION AND STATISTICAL ANALYSIS

Statistical details are given in figure legends. If not otherwise indicated, at least three independent experiments (biological replicates) were performed. Statistical significance was determined using unpaired t test. p values >0.05 were considered as not significant. Data is presented as means ± SD. Statistical analysis was performed using GraphPad Prism (v9.2.0).

Cell Reports, Volume *39*

Supplemental information

Human peroxiredoxin 6 is essential for malaria parasites and provides a host-based drug target

Matthias Paulus Wagner, Pauline Formaglio, Olivier Gorgette, Jerzy Michal Dziekan, Christèle Huon, Isabell Berneburg, Stefan Rahlfs, Jean-Christophe Barale, Sheldon I. Feinstein, Aron B. Fisher, Didier Ménard, Zbynek Bozdech, Rogerio Amino, Lhousseine Touqui, and Chetan E. Chitnis

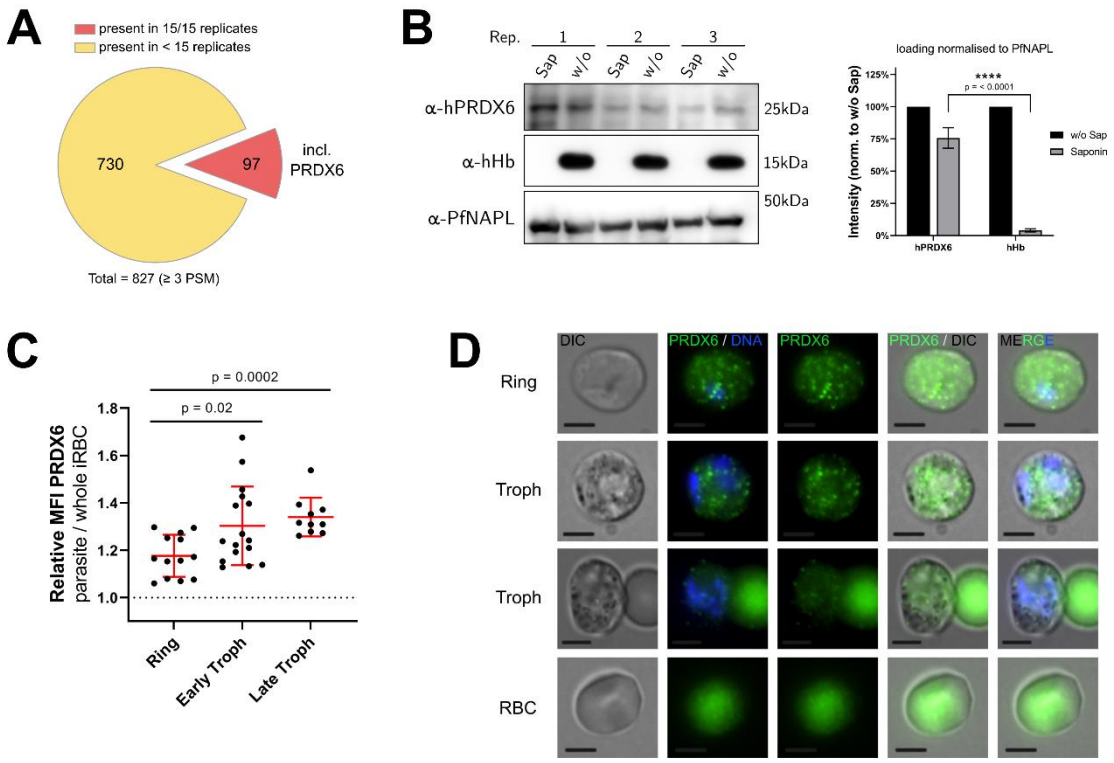

Fig. S1. Host PRDX6 is imported by *P. falciparum and P.* yoelii.

(A) *P. falciparum* infected RBCs were treated with saponin to selectively lyse the RBC membrane. The RBC cytosol was removed by centrifugation. In 15 biological replicates of LC-MS/MS analyses of saponin-liberated mature parasite lysates, 827 human proteins with ≥ 3 peptide spectrum matches (PSM) were detected and were subsequently filtered based on the frequency of occurrence across the 15 sample preparations. Only 97 of these human proteins, including PRDX6, were found in all 15 datasets. The full list of the 97 proteins with abundance information can be found in supplementary table S3. Related to Figure 1 and Table S3.

(B) Immunoblots of saponin-treated and untreated schizonts show localization of human PRDX6 within the parasite. Saponization causes the loss of RBC cytosol proteins such as hemoglobin (Hb). *Pf*NAPL serves as a loading control. Band intensities for human PRDX6 and hemoglobin were quantified with the ImageJ software and normalized to *Pf*NAPL. Abb.: Sap, saponin; w/o, without saponin. Related to Figure 1.

(C) Three dimensional quantification of fluorescent PRDX6 signal in *P. falciparum* infected RBCs. The integrated fluorescence density (IFD) and area of both the parasite as well as the whole infected RBC were measured in multiple z-planes. For each z-plane, the relative IFD of the parasite within the infected RBC was divided by the relative area of the parasite within the infected RBC to calculate the relative mean fluorescent signal located within the parasite as compared to the whole RBC: $(IFD_{Parasite}/IFD_{iRBC})/(Area_{Parasite}/Area_{iRBC})$. The ratio was greater than 1 for all stages and increased from ring stage parasites to late stage trophozoites, indicating that PRDX6 is selectively imported by the parasite. Related to Figure 1A.

(D) Localisation of PRDX6 in *P. yoelii*-infected mouse RBCs. Immuno-fluorescence microscopy shows multiple PRDX6 foci adjacent to *P. yoelii* ring stage parasites. In trophozoites, PRDX6 was also found adjacent to the parasite food vacuoles (FVs) as indicated by small hemozoin crystals. Uninfected mouse RBCs exhibit an even cytosolic staining of PRDX6. DNA, Hoechst 33342 (nuclei). Scale bars: 5 µm. Representative images from three independent experiments. Related to Figures 1A, 2E and 2F.

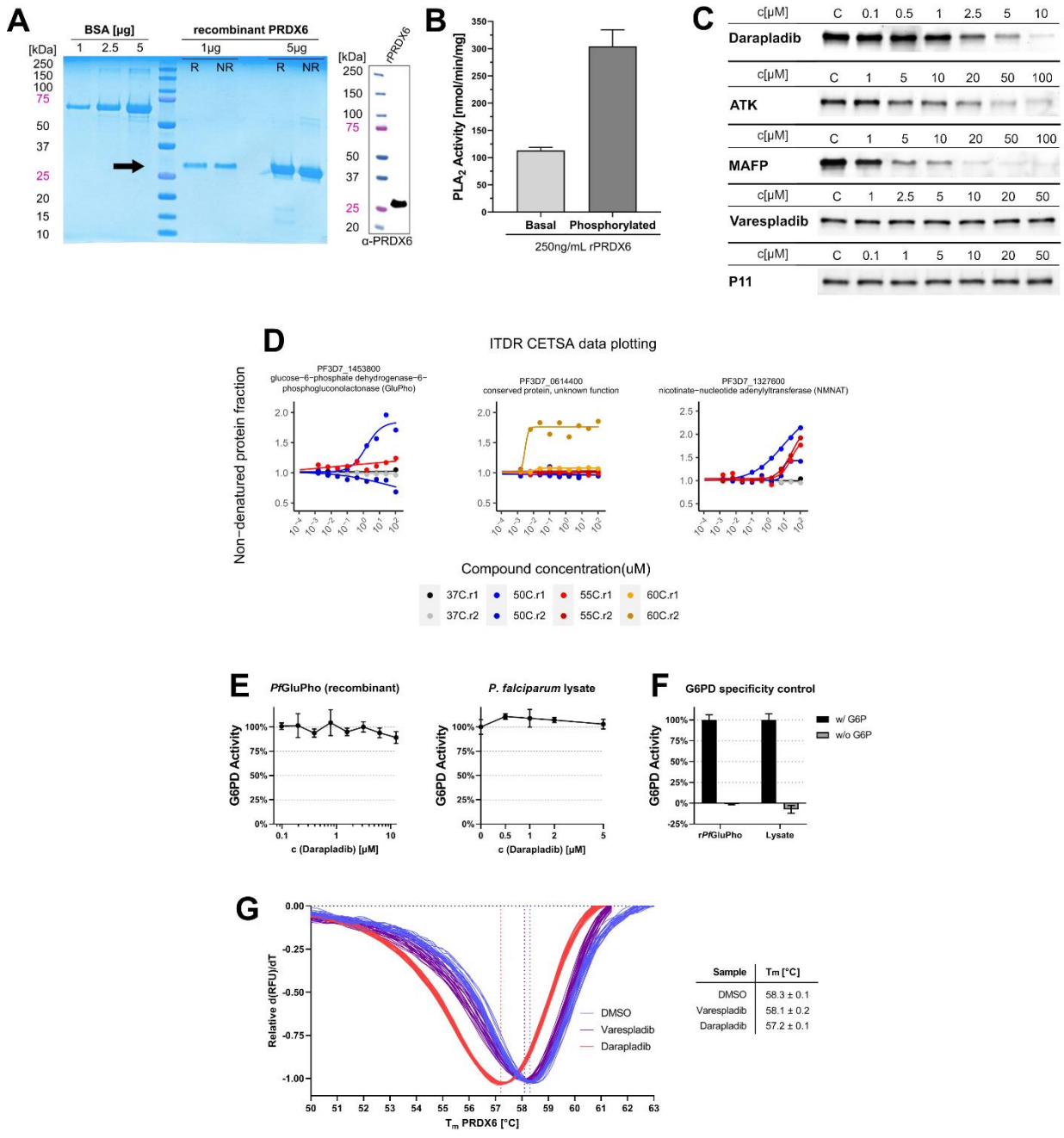

Fig. S2. Expression of PRDX6 and target validation of Darapladib.

(A) Expression and characterization of recombinant PRDX6 (rPRDX6). Purified rPRDX6 migrates as a single band at the expected size of 27 kDa on SDS-PAGE and identity of rPRDX6 was confirmed by immunoblotting with a monoclonal α-hPRDX6 antibody. Related to Figures 2A and 2D.

(**B**) Specific PLA_2 activity of basal and phosphorylated rPRDX6 was consistent with published data (Wu et al., 2009). Related to Figures 2A and 2D.

(C) Activity-based protein profiling: Darapladib, MAFP and ATK, but not Varespladib bind to human PRDX6. Recombinant human PRDX6 was incubated with PLA_2 inhibitors Darapladib, ATK, MAFP, P11 and Varespladib and subsequently labelled with the fluorescent ABPP-probe TAMRA-FP. After SDS-PAGE, the polyacrylamide gel was imaged using a Cy3 filter set. Darapladib, MAFP and ATK, but not Varespladib and P11, reduced labelling of human

PRDX6. This indicates that Darapladib, ATK and MAFP bind to the PLA_2 active site of PRDX6. Representative gels of three independent experiments are shown, full gels are available online, cf. key resources table. Related to Figure 2A.

(D) Thermal stability profile of proteins identified in ITDR-CETSA under Darapladib treatment. Individual stability profiles of hits related to Fig. 2G for the *P. falciparum* proteome. Soluble protein abundance after thermal challenge [50°C (blue), 55°C (red) and 60°C (yellow)] is plotted relative to no-drug control along drug concentration gradient (x-axis). Non-denaturing control (37°C) plotted in black. Data represents 2 independent biological replicates. Related to Figure 2G.

(E) Darapladib does not inhibit the essential glucose-6-phosphate dehydrogenase (G6PD) activity of *Pf*GluPho. The glucose-6-phosphate dehydrogenase (G6PD) activity of recombinant *P. falciparum* glucose-6-phosphate dehydrogenase-6-phosphogluconolactonase (*Pf*GluPho) was measured by quantification of NADPH production. Darapladib does not inhibit the G6PD activity of recombinant *Pf*GluPho or in *P. falciparum* 3D7 lysates. Data are means ± SD of two independent experiments. Related to Figures 2G and S2D.

(F) No G6PD background activity or non-specific NADPH production was detected in control samples which lacked the substrate glucose-6-phosphate. Data are means ± SD of two independent experiments. Related to Figure S2E.

(G) Darapladib, but not Varespladib induces a significant thermal shift in PRDX6. The thermal shift of the melting temperature of PRDX6 in presence of Darapladib and Varespladib was determined using a SYPRO orange-based differential scanning fluorimetry (DSF) assay. $\Delta T_m > 0.5$°C was considered significant. Incubation with 25µM Darapladib decreased the T_m of PRDX6 by 1.1 ± 0.2 °C, while 25µM Varespladib did not significantly change the T_m of PRDX6. Data are individual curves of three independent experiments with nine technical replicates each. Related to Figure 2G.

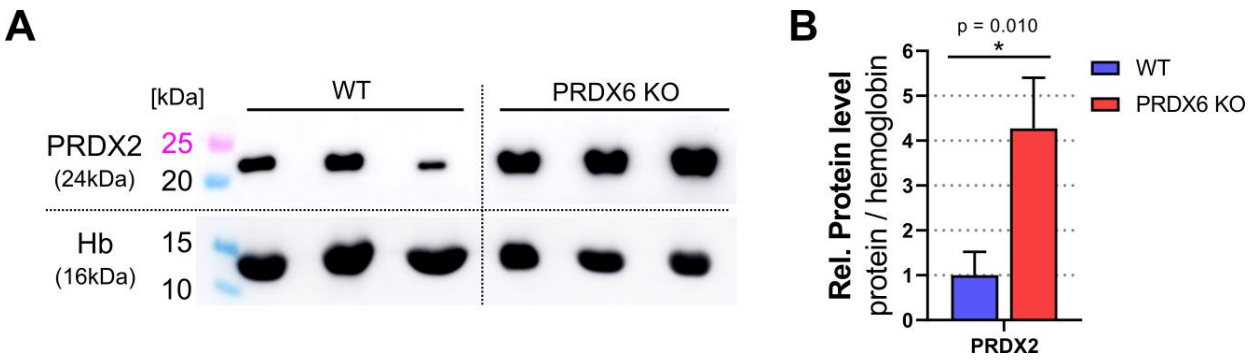

Fig. S3. Loss of PRDX6 induces compensatory overexpression of PRDX2 in mice.

(A) The protein levels of PRDX2 and hemoglobin (control) were determined by immunoblotting of RBCs from each three *prdx6*$^{-/-}$ and WT mice. Related to Figures 2E and 2F.

(B) Bands for PRDX2 from the immunoblot in (A) were quantified and normalized to hemoglobin levels by ImageJ software. Data are means ± SD of three biological replicates, unpaired t-test. Related to Figures 2E and 2F.

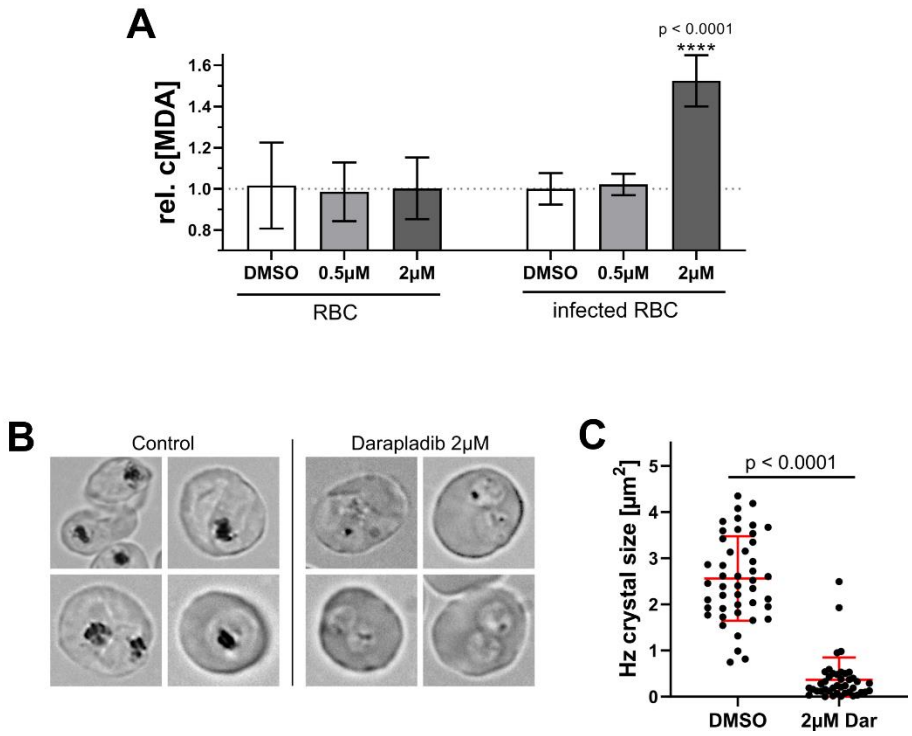

Fig. S4. Darapladib treatment increases oxidative stress and reduces size of hemozoin crystals.

(A) Darapladib treatment increases malondialdehyde (MDA) levels. Treatment of asynchronous *P. falciparum* 3D7 cultures with Darapladib lead to a significant increase of MDA levels in infected RBCs as detected with the TBARS assay. Uninfected RBCs remained unaffected following Darapladib treatment. Data are means ± SD of three independent experiments, unpaired t-test. Related to Figure 2H and I.

(B) Treatment of *P. falciparum* with Darapladib at ring stage decreases hemozoin crystal size. DIC images show that *P. falciparum* 3D7 parasites contain smaller hemozoin crystals following treatment with Darapladib. Representative images from three independent experiments are shown. Related to Figure 3.

(C) The average size of hemozoin crystals from (B) was measured using ImageJ and is greatly reduced by treatment with Darapladib. Data are means ± SD of three independent experiments, unpaired t-test. Related to Figure 3.

SUPPLEMENTARY TABLES

Table S1.

IC_{50} values for several PLA_2 inhibitors for inhibition of *P. falciparum* blood stage progression and growth. Synchronous *P. falciparum* 3D7 culture were treated at ring stage with inhibitors and subsequently allowed to progress to schizont stage ("progression") or to complete the full blood stage cycle until the next generation ring stage ("growth") and measured quantitatively by flow cytometry using SYBR Green I. Data are means ± SD of three independent experiments. ***Abb.:*** *ATK, Arachidonyl trifluoromethyl ketone; MAFP, Methoxy arachidonyl fluorophosphonate.* Related to Figure 2B.

Inhibitor	IC_{50} Progression [µM]	IC_{50} Growth [µM]
Darapladib	0.56 ± 0.02	0.76 ± 0.01
ATK	3.63 ± 0.1	2.14 ± 0.06
MAFP	9.09 ± 0.18	3.86 ± 0.08
Varespladib	No inhibition	No inhibition
P11	No inhibition	No inhibition

Table S2.

Co-treatment with Darapladib and Artemisinin synergistically reduces parasite survival. The data corresponds to Figure 4A in the main text. The survival rate for treatment with 1 µM Darapladib alone and 700 nM DHA alone was multiplied to calculate a theoretical survival rate if the effect of the combination was additive ("Calc. Additive"). The experimentally measured survival rate ("Measured") was divided by the calculated theoretical additive survival rate for the co-treatment. A ratio < 1 for Measured/Calc. indicates synergism, a ratio = 1 indicates an additive effect and a ratio > 1 indicates an antagonistic effect. Data are means ± SD of six independent experiments for NF54 C580Y and three independent experiments for 3815 and 3601, unpaired t-test. Related to Figure 4A.

	Parasite survival				
	Drugs Alone		Combination		Ratio
Strain	Dar 1µM	DHA	Calc. Additive	Measured	Measur./Calc.
NF54 C580Y	89.0 ± 8.1%	7.9 ± 1.7%	7.0 ± 2.1%	0.1 ± 0.3%	0.01 **** (p<0.0001)
3815	94.7 ± 3.2%	7.1 ± 0.9%	6.7 ± 1.1%	3.3 ± 0.5%	0.49 ** (p=0.008)
3601	89.6 ± 6.7%	28.3 ± 3.0%	25.4 ± 4.6%	21.9 ± 2.7%	0.89 ns

Table S3.

PRDX6 is identified in lysates of blood stage *P. falciparum* parasites. *P. falciparum* infected RBCs were treated with saponin to selectively lyse the RBC membrane. 4242 human proteins were detected in LC-MS/MS analyses of saponin-liberated mature parasite lysates in 15 biological replicates. 827 of the human proteins, which were found with ≥3 peptide spectrum matches (PSM), were subsequently filtered based on the frequency of occurrence across the 15 sample preparations. Only 97 of these human proteins, including PRDX6, were found in all 15 datasets. Related to Figures 1 and S1.

ID	Protein Name	[PSM]	Rep1	Rep2	Rep3	Rep4	Rep5	Rep6	Rep7	Rep8	Rep9	Rep10	Rep11	Rep12	Rep13	Rep14	Rep15	Average	stdev
P68871	Hemoglobin subunit beta		1509	1868	1552	1457	1407	1339	797	449	394	699	539	414	547	603	760	**956**	**504**
P69905	Hemoglobin subunit alpha		1638	1347	1327	1118	1484	1384	430	284	306	218	416	175	218	317	484	**743**	**557**
P02042	Hemoglobin subunit delta		901	981	918	884	833	819	479	293	259	367	320	216	347	368	501	**566**	**285**
P02549	Spectrin alpha chain, erythrocytic 1		352	294	306	260	306	319	292	407	384	159	222	146	99	227	292	**271**	**87**
P00915	Carbonic anhydrase 1		374	366	350	341	350	314	262	150	136	140	219	124	349	233	314	**268**	**94**
P04406	Glyceraldehyde-3-phosphate dehydrogenase		360	311	301	269	296	280	297	303	316	122	331	179	158	166	209	**260**	**73**
P04040	Catalase		236	207	193	228	192	192	154	155	149	116	156	118	163	231	257	**183**	**43**
P11142	Heat shock cognate 71 kDa protein		162	194	163	142	164	139	176	238	222	101	155	131	139	174	159	**164**	**35**
Q13228-4	Isoform 4 of Methanethiol oxidase		140	113	117	128	130	130	122	174	160	63	123	78	84	104	123	**119**	**29**
P69891	Hemoglobin subunit gamma-1		219	208	221	200	209	189	42	54	49	46	73	46	43	52	80	**115**	**79**
P11171	Protein 4.1		133	120	121	116	131	121	124	116	106	82	113	76	107	100	135	**113**	**17**
P62979	Ubiquitin-40S ribosomal protein S27a		122	103	107	117	110	98	99	130	119	96	127	97	105	134	115	**112**	**13**
P04264	Keratin, type II cytoskeletal 1		96	126	98	141	86	156	99	89	115	50	122	78	37	88	69	**97**	**32**
P60709	Actin, cytoplasmic 1		106	92	79	72	86	84	92	133	115	52	119	70	70	123	149	**96**	**27**
P32119	Peroxiredoxin-2		90	110	105	104	93	92	61	62	54	75	77	62	148	123	175	**95**	**34**
P00441	Superoxide dismutase [Cu-Zn]		123	115	108	112	100	104	58	101	83	58	73	77	107	78	92	**93**	**20**
P35612	Beta-adducin		100	76	89	81	93	92	107	121	129	64	81	61	84	96	100	**92**	**19**
P0DMV9	Heat shock 70 kDa protein 1B		98	102	84	84	90	89	91	105	97	71	77	80	78	119	95	**91**	**13**
P13645	Keratin, type I cytoskeletal 10		77	96	90	154	68	142	107	81	74	55	99	86	47	90	66	**89**	**29**
P30043	Flavin reductase (NADPH)		111	98	95	71	102	88	47	60	66	51	76	31	78	55	88	**74**	**23**
P60174	Triosephosphate isomerase		74	87	77	78	75	66	70	86	79	48	69	56	63	71	88	**72**	**11**
P07384	Calpain-1 catalytic subunit		73	63	64	57	68	62	81	96	92	51	46	21	81	57	67	**65**	**19**
P35908	Keratin, type II cytoskeletal 2 epidermal		64	66	54	103	58	114	84	48	39	51	82	58	26	66	47	**64**	**23**
P07900-2	Isoform 2 of Heat shock protein HSP 90-alpha		58	54	63	55	61	55	65	63	57	44	51	56	70	77	87	**61**	**11**
P35527	Keratin, type I cytoskeletal 9		49	69	66	71	49	70	55	75	111	32	76	72	21	50	46	**61**	**21**
P13798	Acylamino-acid-releasing enzyme		80	64	63	65	71	65	54	72	79	33	63	37	47	42	67	**60**	**15**
P02730	Band 3 anion transport protein		44	40	35	34	52	47	52	120	125	26	71	54	33	48	107	**59**	**32**
P06753-2	Isoform 2 of Tropomyosin alpha-3 chain		58	58	57	78	61	55	51	78	72	21	48	38	27	54	60	**54**	**16**
P00918	Carbonic anhydrase 2		94	87	90	83	93	76	73	21	24	25	25	18	8	27	38	**52**	**33**
P62258	14-3-3 protein epsilon		62	66	58	52	49	51	52	69	55	42	44	41	34	48	56	**52**	**10**
P02100	Hemoglobin subunit epsilon		94	78	95	78	99	97	18	32	26	19	40	23	23	23	24	**51**	**34**
P02768	Serum albumin		41	63	43	30	31	236	34	18	36	31	61	42	11	43	47	**51**	**53**
P06733	Alpha-enolase		73	48	54	49	59	51	60	39	32	18	53	35	61	57	57	**50**	**14**
P63104	14-3-3 protein zeta/delta		55	59	43	46	43	41	42	70	52	42	52	47	36	57	58	**50**	**9**
P00390	Glutathione reductase, mitochondrial		50	51	47	37	47	50	44	62	60	20	54	42	34	48	39	**46**	**11**
P31946	14-3-3 protein beta/alpha		52	57	45	42	41	38	35	67	47	36	43	39	33	48	47	**45**	**9**
P14625	Endoplasmin		40	40	38	36	40	34	37	66	52	47	50	42	51	45	51	**45**	**8**

Q08495	Dematin	40	45	38	37	47	37	39	49	48	40	41	31	59	45	55	**43**	**7**
P61981	14-3-3 protein gamma	44	57	41	39	38	36	33	64	47	40	40	34	33	42	43	**42**	**9**
P55072	Transitional endoplasmic reticulum ATPase	63	52	51	53	47	52	55	34	25	20	32	17	20	39	45	**40**	**15**
Q06830	Peroxiredoxin-1	51	41	54	52	38	39	28	28	31	31	30	29	32	48	54	**39**	**10**
P40925-3	Isoform 3 of Malate dehydrogenase, cytoplasmic	47	44	38	36	37	33	31	38	39	32	36	37	34	45	45	**38**	**5**
P07195	L-lactate dehydrogenase B chain	63	62	49	48	48	44	39	22	22	11	27	21	21	35	40	**37**	**16**
P23526	Adenosylhomocysteinase	44	40	40	44	46	47	35	30	34	20	37	23	19	40	42	**36**	**9**
P55786	Puromycin-sensitive aminopeptidase	45	33	37	35	42	35	26	40	52	20	42	24	21	26	36	**34**	**9**
P00558	Phosphoglycerate kinase 1	52	51	50	50	54	50	34	17	20	16	23	20	4	28	26	**33**	**17**
P37837	Transaldolase	41	36	31	46	41	34	36	30	32	15	34	25	21	30	38	**33**	**8**
P61970	Nuclear transport factor 2	45	37	35	30	42	35	47	40	46	7	42	14	9	24	35	**33**	**13**
P29144	Tripeptidyl-peptidase 2	51	52	35	30	52	38	46	30	39	10	25	16	7	21	19	**31**	**15**
P02533	Keratin, type I cytoskeletal 14	29	36	33	42	24	57	31	23	45	26	32	35	10	23	15	**31**	**12**
P09104	Gamma-enolase	38	25	33	27	33	23	34	27	18	8	35	24	54	30	34	**30**	**10**
P09493-5	Isoform 5 of Tropomyosin alpha-1 chain	35	37	31	39	31	31	33	32	33	11	26	21	10	31	35	**29**	**9**
P07203	Glutathione peroxidase 1	34	25	30	20	29	22	36	20	20	14	55	33	18	31	31	**28**	**10**
P50395	Rab GDP dissociation inhibitor beta	39	44	40	38	37	33	21	14	16	16	26	14	11	27	40	**28**	**12**
P35579	Myosin-9	37	40	28	31	34	31	42	17	21	19	7	9	4	46	50	**28**	**14**
Q9NY33	Dipeptidyl peptidase 3	39	29	30	27	27	29	30	31	26	11	29	17	21	30	28	**27**	**7**
P00491	Purine nucleoside phosphorylase	42	43	37	37	51	47	21	7	12	4	18	6	12	22	32	**26**	**16**
P09211	Glutathione S-transferase P	29	27	22	24	31	24	16	44	43	6	26	17	29	20	33	**26**	**10**
Q16775	Hydroxyacylglutathione hydrolase, mitochondrial	30	26	34	23	18	35	21	29	26	13	31	18	21	32	27	**26**	**6**
Q13867	Bleomycin hydrolase	28	27	26	28	28	26	22	32	39	9	37	20	13	17	13	**24**	**9**
P36959	GMP reductase 1	25	23	29	21	27	28	22	24	29	14	24	12	23	21	36	**24**	**6**
P07738	Bisphosphoglycerate mutase	45	29	35	34	41	36	29	7	10	9	11	6	7	20	26	**23**	**14**
P62820	Ras-related protein Rab-1A	26	25	26	23	23	22	17	29	29	11	18	18	16	27	25	**22**	**5**
P00492	Hypoxanthine-guanine phosphoribosyltransferase	21	20	28	20	26	25	23	17	16	17	22	12	18	23	32	**21**	**5**
P04632	Calpain small subunit 1	27	26	19	19	19	25	28	27	25	20	16	6	20	17	24	**21**	**6**
Q00013	55 kDa erythrocyte membrane protein	30	25	23	16	16	18	20	22	27	16	26	16	14	18	21	**21**	**5**
Q99497	Protein/nucleic acid deglycase DJ-1	36	40	32	28	30	32	20	6	5	11	10	7	10	20	20	**20**	**12**
P30041	Peroxiredoxin-6	28	26	26	26	24	28	21	6	8	16	10	8	13	22	26	**19**	**8**
P62826	GTP-binding nuclear protein Ran	27	21	24	23	21	27	20	12	18	9	12	14	11	14	33	**19**	**7**
P28289	Tropomodulin-1	29	21	16	19	16	15	21	12	15	17	14	15	10	30	34	**19**	**7**
P48637	Glutathione synthetase	20	22	19	18	22	19	17	20	18	7	20	12	16	23	29	**19**	**5**
P60900	Proteasome subunit alpha type-6	20	17	22	23	24	21	23	17	22	10	15	12	8	24	19	**18**	**5**
P25786-2	Isoform Long of Proteasome subunit alpha type-1	26	21	24	19	24	23	20	11	12	7	12	10	7	16	26	**17**	**7**
P25788	Proteasome subunit alpha type-3	19	17	16	17	19	22	19	16	17	11	19	12	8	21	22	**17**	**4**
P28066	Proteasome subunit alpha type-5	23	19	19	13	30	22	19	18	15	10	13	7	9	14	16	**16**	**6**
P07477	Trypsin-1	15	13	16	17	16	8	13	15	23	15	25	15	12	27	15	**16**	**5**
Q16881	Thioredoxin reductase 1, cytoplasmic	21	20	19	22	17	18	14	19	19	8	15	16	6	15	14	**16**	**4**
O14818	Proteasome subunit alpha type-7	17	14	17	19	20	18	15	11	13	10	17	7	9	21	18	**15**	**4**

Q9BRF8	Serine/threonine-protein phosphatase CPPED1	19	15	15	15	17	15	18	18	20	5	12	8	8	17	15	**14**	**4**
P17174	Aspartate aminotransferase, cytoplasmic	20	17	15	21	19	15	14	8	12	7	16	10	12	13	14	**14**	**4**
P22392-2	Isoform 3 of Nucleoside diphosphate kinase B	22	19	19	20	22	18	15	7	7	6	7	4	7	9	18	**13**	**7**
P28074	Proteasome subunit beta type-5	19	15	18	13	16	13	15	8	14	6	15	9	7	15	12	**13**	**4**
P11586	C-1-tetrahydrofolate synthase, cytoplasmic	14	18	14	14	13	11	13	15	18	9	8	10	5	13	14	**13**	**4**
P20618	Proteasome subunit beta type-1	16	11	11	19	14	11	12	14	16	6	9	12	7	16	12	**12**	**4**
P00568	Adenylate kinase isoenzyme 1	19	17	19	14	16	16	17	7	4	9	8	9	4	6	12	**12**	**5**
P78417	Glutathione S-transferase omega-1	20	16	20	15	14	18	12	7	6	6	5	11	7	7	12	**12**	**5**
P62834	Ras-related protein Rap-1A	12	12	11	13	14	12	9	10	12	5	8	7	8	15	17	**11**	**3**
P53004	Biliverdin reductase A	16	12	16	10	15	12	12	7	10	5	10	9	5	10	12	**11**	**3**
P10599	Thioredoxin	7	13	7	9	13	9	6	11	11	8	10	7	26	8	12	**10**	**5**
Q04760	Lactoylglutathione lyase	15	14	14	13	17	14	9	7	10	4	12	6	5	6	9	**10**	**4**
P11166	Solute carrier family 2, facilitated glucose transporter member 1	9	10	8	7	12	8	9	19	23	7	9	8	4	8	11	**10**	**5**
P35754	Glutaredoxin-1	10	10	7	11	9	8	10	11	10	4	6	4	11	11	25	**10**	**5**
P28072	Proteasome subunit beta type-6	12	13	10	13	13	8	6	8	10	7	4	11	7	11	11	**10**	**3**
Q9UKK9	ADP-sugar pyrophosphatase	12	12	8	8	11	8	7	12	12	6	10	7	4	11	15	**10**	**3**
Q13126-2	Isoform 2 of S-methyl-5'-thioadenosine phosphorylase	12	12	8	6	10	10	6	10	10	6	9	6	6	7	9	**8**	**2**
P12955	Xaa-Pro dipeptidase	12	11	10	7	9	9	10	5	5	5	6	7	6	11	11	**8**	**3**
P63208	S-phase kinase-associated protein 1	12	8	10	7	6	11	10	7	7	4	6	5	5	9	9	**8**	**2**